Fixed-wing UAV Modeling and State Estimation

MCE 4.semester project

MCE4-1029A

Study Board of Energy Technology

Aalborg University

February-May, 2024

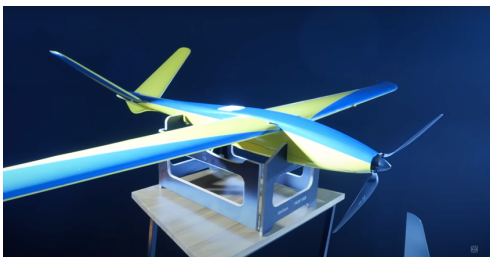

Fifth year at Study board of Energy technology
AAU Energy
Pontoppidanstræde 111
9220 Aalborg
https://www.energy.aau.dk/

Titel:
Fixed-wing UAV
State estimation

Project:
4. Semester MCE

Projektperiode:
February 2024 - May 2024

Author:
Hans Kresten Nørgaard Larsen

Supervisors:
Erik Schaltz

Nr. of pages: 55
Appendix:
Project submitted: May 31, 2024

Abstract:

This project presents two methods of modelling for a fixed-wing mini-UAV. One using only a priori geometric information, and the other relying on the system identification program for aircrafts SIDPAC. The project also develops an airspeed estimate using Field oriented control variables and governing equations for propellers along with experimental data to establish a proof of concept. Both modelling methods are found to be labor intensive to get going, but useful each in its own, once a solution is constructed. Geometric modelling is reliant on knowing the products of inertia and maximum angle of attack as well as non-dimensional lift coefficient at that angle, all of which are not easily obtained. The system identification is most effective if pre-designed input is applied directly to the actuators, to avoid correlation and ensure excitation. Airspeed from FOC was estimated but could not be validated.

Preface

This project has been written by a Mechatronic Control Engineering student. The overall purpose of the project in the 4th semester Mechatronic Control Engineering Master at Aalborg University is to provide experience in solving advanced and relevant engineering tasks.

The student would like to extend a word of thanks to the project supervisor Erik Schaltz for help and guidance throughout the project period.

The in-text citations uses the Vancouver reference style, [Reference number to a given source in the Bibliography].

This semester project was written in LaTeX with calculations and plots made in MATLAB®. Figures were made using Lucidchart.

Hans Kresten Nørgaard Larsen
<hknl19@student.aau.dk>

Nomenclature

Symbol	Definition	Unit
AR	Aspect ratio	[−]
b	Wingspan of UAV	[m]
B_v	Viscous Friction Constant	[Nm · s]
C	Coefficient	[−]
d	Diameter of propeller	[m]
e	Oswald Efficiency factor	[−]
F	Force	[N]
g	Gravitational acceleration	[m/s^2]
h	Altitude	[m]
$\mathbf{H}$	Direct cosine matrix	[−]
i	Current	[A]
J	Advance ratio & Inertia	[−] [kg · m^2]
k	Constant	[−]
K	Temperature	[K]
K_τ	Torque Constant	[RPM/V]
L	Inductance & Axial moments	[H] [Nm]
L_r	Temperature Lapse Rate	[K/m]
m	Mass	[kg]
M	Pitching Moments & Molar mass	[Nm][kg/mol]
n	Rotational Velocity	[rev/s]
n_{pp}	Number of Pole Pairs	[−]
N	Yawing moments	[Nm]
p	Roll rate & Pressure	[rad · s^{-1}] [Pa]
P	Power & Position	[W] [NED]
q	Pitch rate	[rad · s^{-1}]
SM	Static Margin	[m] or [Percent]
Q	Torque	[Nm]
r	Yaw rate	[rad · s^{-1}]
R_s	Phase Resistance	[Ω]
R_u	Universal gas constant	[JK^{-1}mol^{-1}]
S	Surface area	[m^2]
t	Time	[s]
T	Thrust	[N]
u	x-axis Velocity & Control input	[m/s] [−]
U	Voltage	[V]
v	y-axis Velocity	[m/s]
V	Velocity	[m/s]
w	z-axis Velocity	[m/s]
W	Weight	[kgm/s^2]

Symbol	Definition	Unit
x	Translation in x direction & State	[m] [−]
y	Translation in y direction	[m]
Y	Lateral forces	[N]
z	Translation in z direction	[m]
Z	Normal forces	[N]
α	Angle of attack	[rad]
β	Sideslip angle	[rad]
γ	Flight angle	[rad]
Γ	Dihedral angle	[rad]
η	Efficiency	[−]
θ	Pitch Angle	[rad]
λ	Taper ratio & Flux Linkage	[−] [Wb]
Λ	Sweep angle	[rad]
ξ	Heading angle	[rad]
ρ	Air density	[kg/m^3]
τ	Time Constant & Carry over effect	[s] [−]
ϕ	Roll Angel	[rad]
ψ	Yaw Angel	[rad]
ω	Rotational Velocity	[rad $\cdot$ s^{-1}]

Subscripts	Definition
0	Nondependent on α
a,b,c	Phase Indicator
abc	abc-frame
ac	With respect to the aircraft
air	With respect to air
A	Related to Aileron
B	Body frame
cm	With respect to center of mass
cp	With respect to center of pressure
cruise	For cruising flight
d	d-axis
dq0	dq0-frame
D	Drag
DW	Downwash
E	Related to Elevator
i	Lift Induced Drag
I	Inertial frame
F	Related to flaps
Fuselage	Related to fuselage
g	Gravity
h	Altitude dependent
ht	Related to horizontal tail
i	Lift Induced
l	Rolling
L	Lift & Load
p	Parasitic & Component depending on roll rate
prop	Propeller
P	Power
q	q-axis & Component depending on pitch rate
Q	Torque
r	Rotor & Component depending on yaw
R	Related to Rudder
trim	For steady level flight
T	Thrust
tot	Total

Subscripts et alt.	Definition
m	Pitching
max	Maximum
meas	Measured
mech	Mechanical
min	Minimum
mpm	Peak rotor flux linkage
n	Yawing
vt	Related to vertical tail
w	Component depending on shock wave
wa	Wing-aileron relation
W	Wind frame
Wing	Related to wings
xx	Torque application axis and effect axis, similar for yz etc.
X	Axial
Y	Lateral
Z	Normal
α	Component depending on angle of attack
β	Component depending on sideslip angle
δ	Component depending on control deflection
$\bar{X}$	Vector
$\hat{X}$	Nondimensionalized & Estimate
$\dot{X}$	Time derivitive
$\mathbf{X}$	Matrix
X^0	Transition point

Acronym	Definition
AC	AirCraft
AR	Aspect Ratio
BEMF	Back Electromotive Force
BLDC	Brushless Direct Current Motor
CAD	Computer Aided Design
DC	Direct Current
DOF	Degrees Of Freedom
eRPM	Electrical Revolutions Per Minute
ESC	Electronic Speed Controller
FOC	Field Oriented Control
GNSS	Global navigation satellite system
GPS	Global positioning system
IMU	Inertial Measurement Unit
MA	Moving Average
PPM	Pulse Position Modulation
RAF	Relative Airflow
UAV	Unmanned Aerial Vehicle
UI	User Interface
RC	Radio Controlled
RPM	Revolutions Per Minute
SIDPAC	System IDentification Program for AirCrafts
TAS	True Airspeed

Contents

Introduction 1

Up until the 2000s the term "UAV" mostly referred to larger fixwing aircraft's like AAI's RQ series or General Atomics Reaper/Predator program, weighing from 100+ kg to several tons, and with wingspans ranging 5-20 meters. But the use of the hand launchable AeroVironments "RQ-20 Puma" and "RQ-11 Raven" as well as Lockheed Martins "Desert Hawk III" in Iraq and Afghanistan helped solidify the concept of miniature UAVs as payload carrying assets.

The commercial fixed-wing mini-UAVs constructions, propulsion system and control systems are largely similar to those of hobby RC-planes, and both have benefited from the advancements and availability in BLDCs, inverters, lithium batteries and control system ICs, IMUs and open-source flightcontrol software.

Nowadays commercial mini-UAVs are in use for a wider range of applications, such as mapping, wildfire management, search and rescue, police investigation or man-hunt, border control, corporate security/surveillance, ariel photography as well as navel and infrastructure inspection.

The many of-the-shelf options make both the "one off" hobby-build and scaled production relatively streamline. But generic components or sub-assemblies are by definition not optimised for a specific aircraft. For the hobbyist, this is not a huge problem, as the current advancement provides more than sufficient power/precision for short flights without a payload. Commercial production on the other hand, is subject to tighter margins as flight time, range and payload carrying capabilities are the selling point. However as the control system is to be implemented on many identical aircraft from a production-line, a more tailored fit and fine-tuning can be cost effective.

With many of the commercial applications a demand for precise navigation follows, as flights are expected to be longer, out of line-of-sight, semi or fully autonomous. Dependent on the operational setting, the continuous availability of GNSS signal might not be a given. GNSS drop-out could occur due to both terrain, vegetation, large structures or interference, depending on flight altitude or proximity to buildings, metal structures and electrical installation. Direct GNSS-denial is also a plausible scenario for some applications.

This project will address some basic options for increasing robustness of navigation in scenarios where GNSS might not be available.

Problem Analysis 2

This chapter will start off with a short system description of a fixed-wing mini-UAV in general terms. The generic solution for navigation will be presented which includes the rigid-body flat-earth equations of motion, the most common sensors and sensor fusion algorithm. Lastly some options for improving navigation during GNSS signal absence are discussed, leading to the Problem Statement in Chapter 3. If the reader is familiar with the equations of motion, IMU's and Kalman filters they may skip ahead to Section 2.4.

2.1 General System description

Throughout this project the system type in mind will be a light weight, hand launchable fixed-wing aircraft, similar to the "Desert Hawk III", with a wingspan below 3 m and weight below 5 kg.

Figure 2.1. Launching of a Desert Hawk III [10]

Design-wise the these mini-UAVs share some of the same features as regular single prop aircrafts: a pulling propeller at the tip of a streamline fuselage, a set of wings with ailerons, a horizontal tail with an elevator and a vertical tail with a rudder. The airframe is constructed from lightweight materials, usually foamboards, balsa wood or thin plastics in the hobbyists case, but for commercial use more commonly glass-fiber or carbonfiber.

A common drivetrain configuration is two-blade carbon propeller, mounted on the shaft of a BLDC below 1kW, driven by an electronic speed controller (ESC) and powered by a Lithium-ion battery-pack in the 7-30 V range. The control surfaces (aileron, rudder

and elevator) can be actuated through individual servos. The flight controller and radio transceiver can be mounted inside the fuselage along with an Inertial Measurement Unit (IMU). Many flight controller solutions are open-source or community based, and as such need to function for a variety of vehicle designs. The flight controller contains the control and sensorfusion algorithm.

Both the control surface servos and ESC are commonly controlled by a pulse position modulation signal (PPM). In the case of the ESC this is interpreted as the open-loop throttle command for the BLDC. Because most of the available ESCs are generic and designed for BLDCs, the control method is trapezoidal control, as it does not require any prior knowledge of the BLDCs construction, for example number of pole pairs or flux linkage. A simple sketch of the drivetrain is shown in Figure 2.2.

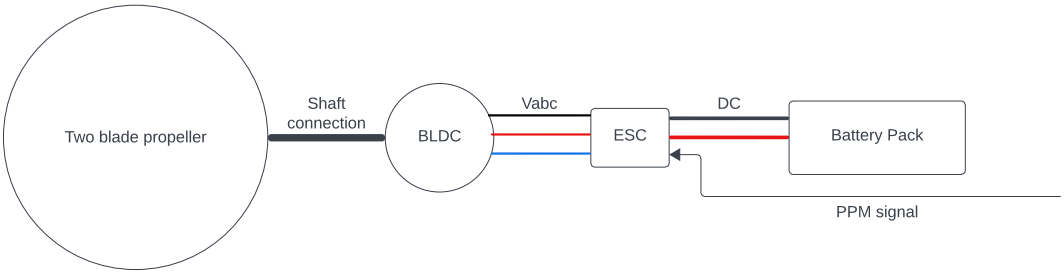

Figure 2.2. Simple illustration of a drivetrain, with throttle command coming from a flight controller

2.2 Flat earth approximation, 6-DOF, rigid body equations of motion

This section will describe the equations of motion for any rigid body object with 6 degrees of freedom. There are many excellent sources for step-by-step derivation, like [8] and [13], just to name a few aircraft related. Therefore this will only be an introduction to the system of equations, which are the typical default for modeling with very little knowledge about the physical system. This general case is what can be expected from at generic off-the-shelf solution that fits many needs and applications.

The equations of motion are functions of the states and inputs, as Equation 2.1.

$$\dot{\bar{x}} = f(\bar{x}, \bar{u}) \tag{2.1}$$

The bar notation $\bar{x}$ denotes a vector in most cases of this project, with the exception of $\bar{c}$ and $\bar{q}$ as will be discussed Chapter 4

The state vector is as shown in Equation 2.2.

$$\bar{x} = \begin{pmatrix} u \\ v \\ w \\ x \\ y \\ z \\ p \\ q \\ r \\ \phi \\ \theta \\ \psi \end{pmatrix} = \begin{pmatrix} \text{velocity component, in x body axis} \\ \text{velocity component, in y body axis} \\ \text{velocity component, in z body axis} \\ \text{position north, inertial reference} \\ \text{position east, inertial reference} \\ \text{position down, inertial reference} \\ \text{roll rate, about x body axis} \\ \text{pitch rate,about y body axis} \\ \text{yaw rate, about z body axis} \\ \text{roll} \\ \text{pitch} \\ \text{yaw} \end{pmatrix} = \begin{pmatrix} x_1 \\ x_2 \\ x_3 \\ x_4 \\ x_5 \\ x_6 \\ x_7 \\ x_8 \\ x_9 \\ x_{10} \\ x_{11} \\ x_{12} \end{pmatrix} \tag{2.2}$$

Where the x, y and z translation and rotation each represent a degree of freedom. As can be noted, two reference frames are used, where the "body frame" is fixed to the rigid body.

The "inertial" reference frame will be the external frame of reference and approximates the earth to be flat and not rotating.

The velocity, position, angular rates and orientation can be denoted as Equation 2.3.

$$\bar{V} = \begin{pmatrix} u \\ v \\ w \end{pmatrix}, \qquad \bar{P} = \begin{pmatrix} x \\ y \\ z \end{pmatrix}, \qquad \bar{\omega} = \begin{pmatrix} p \\ q \\ r \end{pmatrix}, \qquad \Phi = \begin{pmatrix} \phi \\ \theta \\ \psi \end{pmatrix} \tag{2.3}$$

From Newtons second law the translational velocity can be written as Equation 2.4.

$$\begin{pmatrix} \dot{u} \\ \dot{v} \\ \dot{w} \end{pmatrix} = \frac{1}{m}\bar{F} - \begin{pmatrix} p \\ q \\ r \end{pmatrix} \times \begin{pmatrix} u \\ v \\ w \end{pmatrix} \tag{2.4}$$

Or more compact as Equation 2.5.

$$\dot{\bar{V}} = \frac{1}{m}\bar{F} - \bar{\omega} \times \bar{V} \tag{2.5}$$

With $\bar{F}$ being the forces applied in the x, y and z body axis directions. Also from Newton II, the angular velocity, shown in Equation 2.6, relates the inertia and moments applied with respect to the x, y, and z axis, to the change in angular velocity.

$$\begin{pmatrix} \dot{p} \\ \dot{q} \\ \dot{r} \end{pmatrix} = \mathbf{I}^{-1} \left(\bar{M} - \begin{pmatrix} p \\ q \\ r \end{pmatrix} \times \mathbf{I} \begin{pmatrix} p \\ q \\ r \end{pmatrix} \right) \tag{2.6}$$

$$\dot{\bar{\omega}} = \mathbf{I}^{-1}(\bar{M} - \bar{\omega} \times \mathbf{I}\bar{\omega}) \tag{2.7}$$

Here $\mathbf{I}$ is the inertia matrix, which typically can be simplified by some symmetry about an axis, bold indicating that it is a matrix. While $\bar{M}$ is the moments being applied, again in the body frame of reference.

For the change in Euler angles, Equation 2.8 uses a matrix, $\mathbf{C}$, relating the attitude, inertial frame, and on-board measured angular rates, body frame.

$$\begin{pmatrix} \dot{\phi} \\ \dot{\theta} \\ \dot{\psi} \end{pmatrix} = \mathbf{C}(\Phi)\bar{\omega} \tag{2.8}$$

$$\mathbf{C}(\Phi) = \begin{bmatrix} 1 & \tan\theta\sin\phi & \tan\theta\cos\phi \\ 0 & \cos\phi & -\sin\phi \\ 0 & \sin\phi/\cos\theta & \cos\phi/\cos\theta \end{bmatrix} \tag{2.9}$$

The change in translational position can be found using the previous position and direction cosine matrix, $\mathbf{H}(\Phi)$.

$$\dot{\bar{P}} = \bar{V}_I = \mathbf{H}(\Phi)\bar{V}_B \tag{2.10}$$

So $\mathbf{H}$ is the transformation matrix form the inertial reference frame to the body frame of reference, shown in Equation 2.11.

$$\mathbf{H}(\Phi) = \begin{bmatrix} cos(\theta)cos(\psi) & cos(\theta)sin(\psi) & -sin(\theta) \\ sin(\phi)sin(\theta)cos(\psi) - cos(\phi)sin(\psi) & sin(\phi)sin(\theta)sin(\psi) + cos(\phi)cos(\psi) & sin(\phi)cos(\theta) \\ cos(\phi)sin(\theta)cos(\psi) + sin(\phi)sin(\psi) & cos(\phi)sin(\theta)sin(\psi) - sin(\phi)cos(\psi) & cos(\phi)cos(\theta) \end{bmatrix} \tag{2.11}$$

Unlike $\mathbf{C}$, $\mathbf{H}$ can be transposed to reverse the transformation.

The generic model can be compactly written as in Equation 2.12

$$\dot{\bar{x}} = \begin{pmatrix} \frac{1}{m}\bar{F} - \bar{\omega} \times \bar{V}^b \\ \mathbf{H}(\Phi)\bar{V}^b \\ \mathbf{I}^{-1}(\bar{M} - \bar{\omega} \times \mathbf{I}\bar{\omega}) \\ \mathbf{C}(\Phi)\bar{\omega} \end{pmatrix} \tag{2.12}$$

The definition of m, $\mathbf{I}$, $\bar{F}$ and $\bar{M}$ is then vehicle specific.

The control input vector is also vehicle specific, but in a simple form, a scaling or mapping of the throttle command can be interpreted as a force application in the x body direction.

$$\bar{u} = (\delta\text{thtl}) = (\text{throttle command}) \tag{2.13}$$

The complexity or precision of the model now depends on the definition of the components of $\mathbf{I}$, $\bar{F}$ and $\bar{M}$. The forces applied can be expressed as the sum of different sources, as in Equation 2.14.

$$\bar{F} = \bar{F}_g + \bar{F}_B \tag{2.14}$$

With $\bar{F}_g$ being the gravitational force, normally defined as positive in the positive z direction of the inertial frame (down), and $\bar{F}_B$ being the remaining modeled forces on the vehicle. The latter follows the vehicle body frame, but the gravitational part should be a transformation from inertial to body frame using $\mathbf{H}$. The same goes for the moments acting on the vehicle, but if the center of gravity is chosen as reference, the gravitational moments are zero.

2.3 IMU

To measure the vehicle attitude or orientation, a collection of sensors known as an Inertial measurement unit (IMU) is commonly used. Through measurements, the orientation of the inertial and body reference frames with respect to each other can be determined and used for states in the vehicle model as described in the previous section.
An IMU contains a number of gyroscopes, accelerometers and magnetometers for angular rate, acceleration and magnetic field orientation measurements respectively.
Roughly speaking, the inertial reference frame can be determined through the cross product of the measurement of the earths magnetic-field "north", and gravitational acceleration direction. While integration of the angular rate can provide information about the orientation of the vehicle.
But as no sensor is perfect, a combination of these three measurements are used to overcome the individual weaknesses of the sensors. On their own, and without calibration, the sensors are prone to either drift, disturbance or bias.
An off-the-shelf flight controller usually prepossesses the IMU readings to improve accuracy and output the desired states as well as implements the sensor fusion algorithm. Different sensor fusion algorithms could be used, but a Kalman filter is commonly utilized. IMU implementations are very common in a wide range of applications, and are not dependent on vehicle dynamics, as such, the available commercial solutions are deemed sufficiently precise as long as the system is calibrated and adjusted for bias. Therefore, for the remainder of the project, the IMU and sensor fusion algorithm output will be used as is, with the corresponding error covariance.
To iterate, from the IMU and sensor fusion algorithm the inertial reference frame, acceleration, angular rates (x_7, x_8 and x_9) and attitude (x_{10}, x_{11} and x_{12}) are determined. The flight controller solutions is also expected to calculate the angle of attack and sideslip angle, given an accurate velocity vector and attitude measurement.

2.4 Navigation and sensors

As explained in the section above, the Kalman filter can be used to combine measurements in an optimal way. For many applications the IMU readings and GPS signals are used in combination with another form of speed sensor. In a car, this could be an odometer, which measures the wheel rotations. This can increase the accuracy of the position estimate, if the GPS signal is to drop out. Like wise in aviation, regular planes are usually fitted with one or more pitot-tubes which measures the dynamic pressure and thereby the airspeed. In the case of mini-UAVs however the use of pitot tubes is not common, partly because of weight conservation, but mostly because of reliability issues. Pitot-tube are known to have clogging issues due to either dust, insects, moisture or icing. Therefore redundant sensors and/or fault detection is necessary to avoid a crash. Suggestions for a fault detection solution can be found in [3].

For a GNSS-denied scenario mainly two solutions have shown promise.
The use of radio beacons, or Phased arrays is shown by [11] to be a viable backup system, but by definition it requires external installations to function and could be vulnerable to countermeasures.

The other solution for navigation is to have a downward facing camera and match images to a map, also called Simultaneous Localisation and Mapping (SLAM). This solution has been widely utilized and is described by numerous sources, including [6]. But this obviously requires both a camera and the continuous processing of images.

2.5 Summary

As a quick summary it has been discussed that for commercial product it is expected that more time can be put into acquiring information about the aircraft compare to single production systems. The general 6-DOF model in theory describes the movement of a vehicle in 3d space, but without inclusion of aerodynamic forces and moments due to the airframe shape and control surface deflection, the error covariance must then be expected to be relatively wide. The off-the-shelf flight controller, IMU measurement, pre-processing and filtering is expected to have little margin for improvement, without an increase in sensors.
The BLDC control algorithm is separate from the flight controller and usually running Trapezoidal control. Without a pitot tube or GPS signal a speed estimate is reliant on the integral of accelerometer measurements and is not expected to be highly accurate.

The addition of more sensors in the UAV will undoubtedly increase the total weight and unreliability of the completes system, while the use of beacons or image processing are seen as solid solutions but is preferred not used if possible, as they expose weaknesses or higher demands for the UAV.

Problem formulation 3

As has been discussed in the Problem analysis, navigation without GNSS is not impossible but most current solutions depend on the addition of other sensors or external sources of information. For this project the focus will be on improving precision of "weightless" solutions, meaning extending the use of sensors already included in the UAV as part of the drivetrain and flight controller package. Most of the project will however be concerned with expanding the basic vehicle model to something more representative of the real system.
A model expansion is an addition which does not introduce weight or possible mechanical failure point to the UAV, and therefore preferred. The angle of this project will be to include knowledge of the system along with measurements and actuation-commands to reduce the expected error in state estimation.

In the remainder of this short chapter the Problem statement will be presented, followed by an outline of the workflow and scope of the project. Finally, some of the system characteristics, of the UAV used for verification, will be outlined.

3.1 Problem Statement

The main Problem Statement for this project is:

How can a fixed-wing mini-UAV be modeled for more confidence in predicting dynamic behaviour than a generic 6DOF rigid body model?

As a secondary objective the following will also be investigated:

What states can be attained by exploiting information from the drivetrain control algorithms, specifically Field Oriented Control on a BLDC?

3.2 Workflow

Through out this project the following perspectives will be addressed in the listed order:

- How can a parametric model of a mini-UAV be derived from aerodynamic principles and geometric information?
- How can the settings which provide the most efficient cruise flight be found?
- How can a mini-UAV be modeled using system identification methods?
- How can FOC variables be used to aid the flight controller?

For the parametric modelling a detailed CAD drawing and physical measurement will be used to define an aerodynamic model as for full scale aircrafts. With variables from the aerodynamic model, trim minimum-thrust flight conditions will be derived, again using equations from regular aviation.
For the system identification approach, a NASA software package will be utilized with measurements and recorded flight data. After the modelling, the validity of FOC on a BLDC will be presented followed by the use of experimental data to estimate a relation between current, rotor speed and true airspeed.

3.3 Scope of project

As the physical parameters of the case UAV are not the focus of this project, they will not be included. Additionally as the UAV is a commercial product, data restrictions apply. The modeling part of the project will by no means be an exhaustive explanation of how to model Unmanned Aerial Vehicles, but rather an attempt at simplifying the general equations for the specific fixed-wing mini-UAV as much as possible.

3.4 Case UAV

To enable later model-validation against measurement datasets, a working UAV platform is used. Physical parameters are taken from a detailed CAD model of the UAV, or assumed. Flight-logs and other measurements used are naturally also from the same UAV. Voltage, current and rotor speed is recorded separately from the flight control data-logger which produces ulog files for each flight. The case-UAV is a hand launchable fixed-wing system with a single pulling propeller at the nose, just as described in the Problem Analysis. A few features that are relevant for the modelling and signal interpretation is that flaps and ailerons are not separate, but one unit. As such, asymmetric deflections will be counted at aileron deflections, while symmetric deflections will count as flaps in the signal interpretation. Like wise, as the elevator is an all moving tail, what is otherwise known as stabilator input will be the same as elevator input.

Aerodynamic model 4

This chapter will include the aerodynamic model specific equations and geometric measurements used to expand the system model. The solution is based on the course material for "Aircraft Flight Dynamics" by Robert F, Stengel at Princeton University [14].

As the aircraft is expected to performer relatively large ranges of motion but with no change in mass, its dynamics is expected to be covered by Nonlinear time-invariant model for maneuvering. But when cruising an LTI model might suffice[14].

The objective is to establish equations for the forces and moments that are imposed on the system through the aerodynamics due to the aircraft geometry, control surface deflection and operational conditions. In short, Equation 2.14 and its equivalent equation for the Moment are to include aerodynamic effects as these typically dominate the equations of motion[7].

In the first part of this chapter an overview is presented to establish the structure of the model expansion. Then some of the aircraft specific principles are explained, followed by an explanation to the individual non-dimensional aerodynamic coefficients and their components. The result of this chapter will be summerised in Section 4.5

4.1 Structure

The model structure for the aerodynamic model is the same as presented in Section 2.2, which means that the transformations and relations are still applicable. The state-transition for $\bar{P}$ and Φ are therefore unchanged, but for $\bar{\omega}$ and $\bar{V}$ the state-transition is different with the addition of aerodynamics to $\bar{F}$ and $\bar{M}$ as well as changes to $\mathbf{I}$.

4.1.1 Forces and Moments

Besides the gravitational force, the forces and moments from thrust and aerodynamics will be included in the model as seen in Equation 4.1 and 4.2.

$$\bar{F_B} = \begin{bmatrix} X_{aero} + X_{thrust} \\ Y_{aero} + Y_{thrust} \\ Z_{aero} + Z_{thrust} \end{bmatrix}_B = \begin{bmatrix} C_{X_{aero}} + C_{X_{thrust}} \\ C_{Y_{aero}} + C_{Y_{thrust}} \\ C_{Z_{aero}} + C_{Z_{thrust}} \end{bmatrix}_B \frac{1}{2}\rho V^2 S = \begin{bmatrix} C_X \\ C_Y \\ C_Z \end{bmatrix}_B \bar{q}S \tag{4.1}$$

$$\bar{M_B} = \begin{bmatrix} L_{aero} + L_{thrust} \\ M_{aero} + M_{thrust} \\ N_{aero} + N_{thrust} \end{bmatrix}_B = \begin{bmatrix} (C_{l_{aero}} + C_{l_{thrust}})b \\ (C_{m_{aero}} + C_{m_{thrust}})\bar{c} \\ (C_{n_{aero}} + C_{n_{thrust}})b \end{bmatrix}_B \frac{1}{2}\rho V^2 S = \begin{bmatrix} C_l b \\ C_m \bar{c} \\ C_n b \end{bmatrix}_B \bar{q}S \tag{4.2}$$

The directions of these forces and moments are illustrated in Figure 4.1.

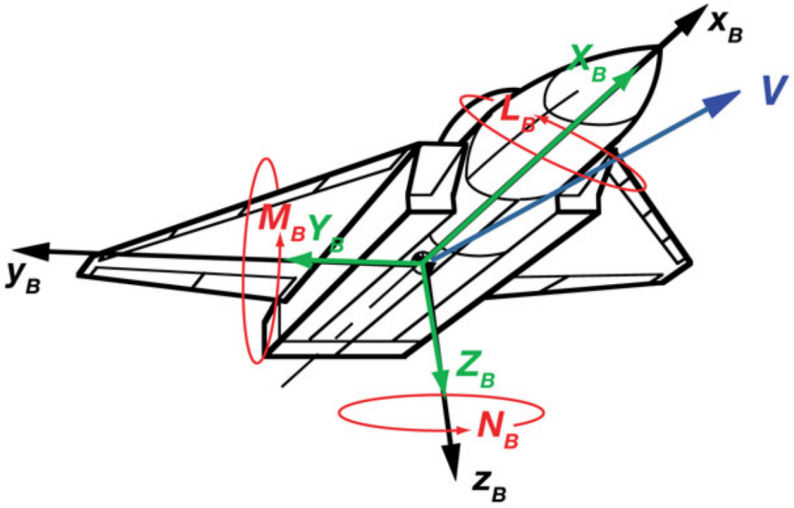

Figure 4.1. The directions of forces and moments in the body frame [14]

The forces and moments in their respective directions can be calculated using non-dimensional aerodynamic coefficients C and the lift equation, which will be elaborated on in Section 4.2.
When related to the air-stream, (aligned with the velocity vector), the force coefficients are the drag, side force and lift coefficients.

$$\bar{F_W} = \begin{bmatrix} C_D \\ C_Y \\ C_L \end{bmatrix}_W \bar{q}S \tag{4.3}$$

4.1.2 Inertia matrix

For an aircraft which is mirror symmetric in the xz-plane, the inertia matrix is simplified as shown i Equation 4.4.

$$I = \begin{bmatrix} I_{xx} & -I_{xy} & -I_{xz} \\ -I_{xy} & I_{yy} & -I_{yz} \\ -I_{xz} & -I_{yz} & I_{zz} \end{bmatrix} \Rightarrow \begin{bmatrix} I_{xx} & 0 & -I_{xz} \\ 0 & I_{yy} & 0 \\ -I_{xz} & 0 & I_{zz} \end{bmatrix} \tag{4.4}$$

Here I_{xz} might also be equal to 0, depending on the nose alignment in relation to the center of mass. In this project I_{xz} is retained.

4.1.3 State-transition function

Specifying $\bar{\dot{x}}$ in Equations 2.4- 2.10 with the use of F_B, M_B and the simplified **I** now looks as presented in Equations 4.5-4.17.

$$\dot{u} = X/m - gsin\theta + rv - qw \tag{4.5}$$
$$\dot{v} = Y/m + gsin\phi cos\theta - ru + pw \tag{4.6}$$
$$\dot{w} = Z/m + gcos\phi cos\theta - qu + pv \tag{4.7}$$
$$\dot{x} = (cos\theta cos\psi)u + (-cos\phi sin\psi + sin\phi sin\theta cos\psi)v + (sin\phi sin\psi + cos\phi sin\theta cos\psi)w \tag{4.8}$$
$$\dot{y} = (cos\theta sin\psi)u + (cos\phi cos\psi + sin\phi sin\theta sin\psi)v + (-sin\phi cos\psi + cos\phi sin\theta sin\psi)w \tag{4.9}$$
$$\dot{z} = (-sin\theta)u + (sin\phi cos\theta)v + (cos\phi cos\theta)w \tag{4.10}$$
$$\dot{p} = \frac{I_{zz}L + I_{xz}N - \{I_{xz}(I_{yy} - I_{xx} - I_{zz})p + [I_{xz}^2 + I_{zz}(I_{zz} - I_{yy})]r\}q}{(I_{xx}I_{zz} - I_{xz}^2)} \tag{4.11}$$
$$\dot{q} = \frac{M - (I_{xx} - I_{zz})pr - I_{xz}(p^2 - r^2)}{I_{yy}} \tag{4.12}$$
$$\dot{r} = \frac{I_{xz}L + I_{xx}N - \{I_{xz}(I_{yy} - I_{xx} - I_{zz})r + [I_{xz}^2 + I_{xx}(I_{xx} - I_{yy})]p\}q}{(I_{xx}I_{zz} - I_{xz}^2)} \tag{4.13}$$
$$\dot{\phi} = p + (qsin\phi + rcos\phi)tan\theta \tag{4.14}$$
$$\dot{\theta} = qcos\phi - rsin\phi \tag{4.15}$$
$$\dot{\psi} = (qsin\phi + rcos\phi)sec\theta \tag{4.16}$$
$$\tag{4.17}$$

From Equations 4.1 or 4.3 and 4.2 along with state-transition Equations it can be seen that aside from the states, the items below are variables that must be defined. Many of which have sub-components as also noted below the relevant items.

- **I** - The inertia matrix (constant)
- m - The total mass (constant)
- S - Wing reference area (constant)
- ρ - Air density
- V - Airspeed
- $\bar{q}$ - Dynamic pressure
- C_T - Thrust coefficient
- C_D - Drag coefficient
  C_{D_α} - ...due to angle of attack
  C_{D_p} - ...Parasitic
  C_{D_w} - ...Wave
  C_{D_i} - ...Lift induced
  $C_{D_{\hat{q}}}$ - ...due to pitch rate

- C_Y - Sideforce coefficient
  C_{Y_β} - ...due to sideslip angle
  $C_{Y_{\hat{q}}}$ - ...due to pitch rate
  $C_{Y_{\hat{r}}}$ - ... due to yaw rate
  $C_{Y_{\delta A}}$ - ...due to Aileron deflection
  $C_{Y_{\delta R}}$ - ...due to Rudder deflection

- C_L - Lift coefficient
  $C_{L_{ht}}$ - ...from horizontal tail
  C_{L_α} - ...due to angle of attack
  $C_{L_{\delta E}}$ - ...due to Elevator deflection
  $C_{L_{\delta F}}$ - ... due to Flaps deflection
  $C_{L_{\hat{q}}}$ - ... due to pitch rate

- C_l - Rolling moment coefficient
  C_{l_β} - ...due to sideslip angle
  $C_{l_{\beta_{Wing}}}$ - ... from wing due to sideslip angle
  $C_{l_{\beta_{Wing-fuselage}}}$ - ...from wing-fuselage interface due to sideslip angle
  $C_{l_{\beta_{vt}}}$ - ... form vertical tail due to sideslip angle
  $C_{l_{\delta A}}$ - ... due to Aileron deflection
  $C_{l_{\delta R}}$ - ... due to Rudder deflection
  $C_{l_{\hat{q}}}$ - ... due to pitch rate
  $C_{l_{\hat{r}}}$ - ... due to yaw rate

- C_m - Pitching moment coefficient
  C_{m_α} -... due to angle of attack
  C_{m_0} - static pitching moment coefficient
  $C_{m_{\delta E}}$ - ... due to Elevator deflection
  $C_{m_{\delta F}}$ - ... due to Flaps deflection
  $C_{m_{\alpha_{ht}}}$ - ... due to angle of attack on the horizontal tail
  $C_{m_{\hat{q}}}$ - ... due to pitch rate

- C_n - Yawing moment coefficient
  $C_{n_{\delta R}}$ - ... due to Rudder deflection
  C_{n_β} - ... due to sideslip angle
  $C_{n_{\beta_{vt}}}$ .. form vertical tail due to sideslip angle
  $C_{n_{\beta_{Fuselage}}}$ - ...from fuselage due to sideslip angle
  $C_{n_{\beta_{Wing}}}$ - ...from wing due to sideslip angle
  $C_{n_{\hat{q}}}$ - ... due to pitch rate
  $C_{n_{\hat{r}}}$ - ... due to yaw rate
  $C_{n_{\delta R}}$ - ... due to Rudder deflection
  $C_{n_{\delta A}}$ ... due to Aileron deflection

The Equations for these variables will be presented in Sections 4.3.1 and 4.4

4.2 General aircraft concepts and equations

Before diving into the explanation of the aerodynamic coefficients some general concepts and equations will be established. The definitions might seam out of context but will be relevant later.

The longitudinal variables are the axial (u) and normal (w) velocity, the velocity (V), angle of attack(α), flight path angle (γ) and pitch (θ).

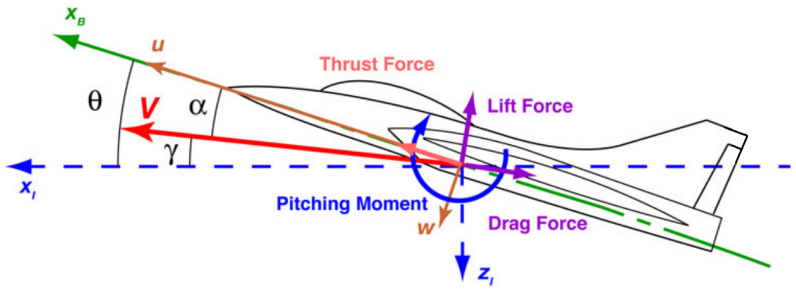

Figure 4.2. Longitudinal variables [14]

The lateral variables are sideslip angle (β), yaw (ψ), roll (ϕ) and heading angle(ξ).

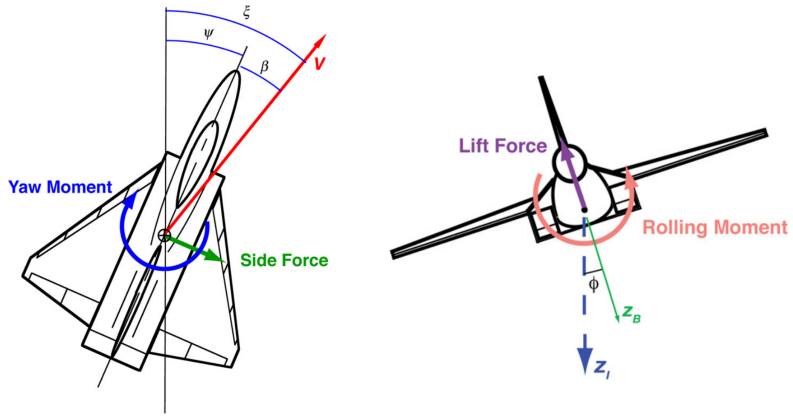

Figure 4.3. Lateral variables [14]

The condition "steady level flight" referes to flight with no change in speed or altitude and is simply called "trim"-conditions, the dynamics of trim flight will be discussed in Section 4.6.

The dynamic pressure $\bar{q}$, not a vector, can be calculated from the air density and airspeed as per Equation 4.18.

$$\bar{q} = \frac{1}{2}\rho(h)V_{air}^2 \tag{4.18}$$

The airspeed is defined as the combination of the x, y and z components.

$$V_{air} = [v_x^2 + v_y^2 + v_z^2]_{air}^{1/2} = [v^T \ v]_{air}^{1/2} \tag{4.19}$$

The True Airspeed (TAS), is the airplanes velocity with respect to the air mass that surrounds it. Therefore the ground speed, in a flat earth approximation, will be TAS minus the wind velocity.

The air density $\rho(h)$ is for the most part dependent on temperature and pressure, both of which change with altitude. An altitude dependent temperature function can be expressed as Equation 4.20 [15].

$$K = K_0 - L_r h \tag{4.20}$$

Here h is the altitude, L_r the temperature lapse rate, $0.0065\,\mathrm{K/m}$, K_0 the temperature at sea level and K is the expected temperature at that altitude. Likewise an altitude dependent function for the pressure can be expressed as Equation 4.21.

$$p_h = p_0(1 - \frac{L_r h}{K_0})^{\frac{gM}{R_u L_r}} \tag{4.21}$$

Here g is the gravitational acceleration at sea level, M is the molar mass of dry air, $0.028\,97\,\mathrm{kg/mol}$, R_u is the universal gas constant, p_0 is the pressure at sea level and p_h the expected pressure the given altitude. These two equation can then be combined in the ideal gas law as Equation 4.22.

$$\rho(h) = \frac{p_0 M}{R K_0}(1 - \frac{L_r h}{K_0})^{\frac{gM}{RL_r}-1} \tag{4.22}$$

$$\rho(h) = \frac{p_h M}{R_u K} \tag{4.23}$$

The dynamic pressure is used extensively throughout the modelling, because it is a part of the general lift equation. Lift, as shown in Equation 4.24, is calculated as a relation between the reference area S and the dynamic pressure along with the non-dimensional lift coefficient, C_L.

$$Lift = C_L \frac{1}{2}\rho(h) V_{air}^2 S \tag{4.24}$$

The coefficient C_L can be separated into components as will be discussed in Section 4.3.1.

On the case-UAV the source of propulsion is the two blade propeller, therefore the thrust Equation 4.25 looks just like the lift equation, as it is essentially a fast rotating wing.

$$Thrust = C_T \frac{1}{2}\rho V^2 S_{prop} \tag{4.25}$$

It should be noted that here the reference area is the propellers own surface area.

An angular change of the aircraft is done about the center of mass with the force being applied at the center of pressure.

The static margin (SM) is the body frame x-axis distance between the center of pressure and the center of mass for the aircraft, as shown in Figure 4.4.

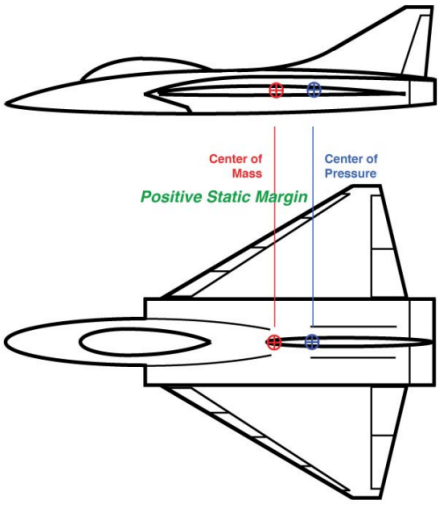

Figure 4.4. An example of the static margin [14]

SM can be normalized, h, with $\bar{c}$ like in Equation 4.26.

$$SM = \frac{100(x_{cm} - x_{cp})_B}{\bar{c}} \equiv 100(h_{cm} - h_{cp}) \tag{4.26}$$

Remembering that $\bar{c}$ is the mean aerodynamic chord length (not a vector).

For a symmetric wing, the center of pressure is located at 1/4 from the leading edge of the mean aerodynamic chord (mac). This contributes to the airframes center of pressure.

The aspect ratio, AR, can be calculated as in Equation 4.27.

$$AR = \frac{b^2}{S} \tag{4.27}$$

With b being the wingspan and S the wing area, which in this project is also the reference area.

4.3 Longitudinal Forces

This section will describe the force and moment coefficient which govern the movement in the xz-plane. Movements are of course coupled but will be described separately. The additions to the modeled forces and moments mostly come from the aerodynamics, for which the lift equation has already been presented. The short and general form is as seen in Equation 4.28.

$$F = C\bar{q}S \tag{4.28}$$

Where F and C will be different depending on the context, but all the components will be normalised to the same dynamic pressure and reference area S. This enables a more compact notation in the end, but the bookkeeping along the way will not be minute. It is important to note that C is a coefficient, not a constant, as it depends on angle of attack among other variables and will be modeled as Look Up Tables, LUT.

4.3.1 Lift and Drag

Starting off with the lift, as shown in Equation 4.29, depends on angle of attack and other variables, as just discussed.

$$C_L \approx C_{L_0} + \frac{\partial C_L}{\partial \alpha}\alpha \tag{4.29}$$

The lift coefficient is separated into components, where C_{L_0} is the lift which is not dependent on angle of attack, and its contributors are the wings and horizontal tail as shown in Equations 4.30 to 4.32

$$C_{L_{Wing}} = \frac{\pi AR}{1 + \sqrt{1 + \left(\frac{0.5AR}{cos\Lambda_{1/4wing}}\right)^2}} \tag{4.30}$$

$$C_{L_{ht}} = (1 - k_{DW})\frac{\pi AR_{ht}}{1 + \sqrt{1 + \left(\frac{0.5AR}{cos\Lambda_{1/4ht}}\right)^2}}\frac{S_{ht}}{S}, \qquad k_{DW} = \frac{C_{L_{Wing}}}{\pi eAR} \tag{4.31}$$

$$C_{L_0} \approx C_{L_{Wing}} + C_{L_{ht}} \tag{4.32}$$

With $\Lambda_{1/4wing}$ being the sweep angle at 1/4 distance from fuselage to wing tip and $\Lambda_{1/4ht}$ the quarter sweep angle for the horizontal tail, shown in Figure 4.5. While k_{DW} is the down-wash sensitivity. Lift from the fuselage is not included in this particular model.

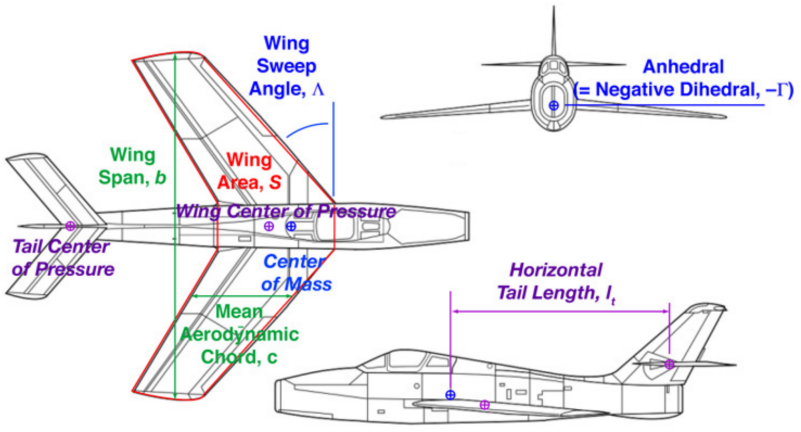

Figure 4.5. Illustration of some of the measurements used in the following sections [14]

To approximate the α-dependent lift coefficient it is divided in to three parts.
The first part is selected to cover angle of attack from $-10 - +18°$ and is calculated as Equation 4.33.

$$C_{L_{\alpha(-10-+18)}} = C_{L_{max}} \ sin\left(\frac{\pi}{2}\frac{\alpha}{\alpha_{max}}\right) \tag{4.33}$$

Where the maximum lift coefficient, $C_{L_{max}}$, is set to 1.9 and the maximum α to 20°. Values were chosen from experimental data for similar airfoils, in this case from [4]. This will be the first and linear part of the lift curve, called the lift curve slope.
The second part is for transition from lift curve slope and passing the stall angle of attack, here a cubic fit can be made. The two points, transition (α^0, $C_{L_{trans}}$) and the peak (α_{max},C_{L_max}) are used along with zero slope at the max point. Transition angle, α^0, is chosen two degrees below α_{max}.

For the third part, a Newtonian approximation is made. For Newtonian flow the normal force N on the aircraft which has components lift and drag, is the product of mass-flow over area, change in velocity, projected area and angle between "plate" and velocity (α). This can be expressed as Equation 4.34.

$$\begin{aligned} N =& (\rho V)(V-0)(S\sin\alpha)(\sin\alpha) = (\rho V^2)(S\sin^2\alpha) \Rightarrow \\ =& (2\sin^2\alpha)(\frac{1}{2}\rho V^2)S \equiv C_N \bar{q} S \end{aligned} \tag{4.34}$$

$$C_N = 2sin^2\alpha \tag{4.35}$$

Then the lift and drag components can be found by projecting N as in Equation 4.36.

$$\begin{aligned} Lift = Ncos\alpha, \quad C_L = C_N cos\alpha \\ Drag = Nsin\alpha, \quad C_D = C_N sin\alpha \end{aligned} \tag{4.36}$$

As all coefficient converge to Newtonian like values, the Newtonian approximation of the lift coefficient $C_{L_{Newton}}$ is used for the third part, up to 90° angle of attack, as seen in Equation 4.37

$$C_{L_{Newton}} = \left(2sin^2\alpha \ sign(\alpha)\frac{S_{plan}}{S}\right) cos\alpha \tag{4.37}$$

Where S_{plan} is the shadow area of the aircraft which is used to normalise $C_{L_{Newton}}$. The calculated lift coefficient versus angle of attack is shown in Figure 4.6

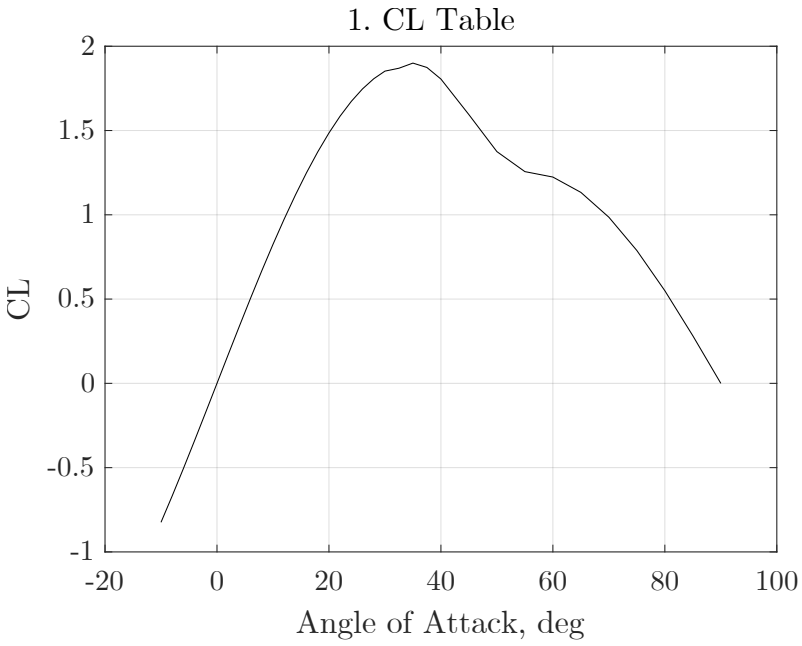

Figure 4.6. The calculated lift slope with angle of attack for the case-UAV

The remaining coefficients will have similar curves, but will not be shown. If however non of the points are known, the lift curve slope can be found as by Equation 4.38 for aspect ratio larger than 5, which the case-UAV has.

$$C_{L_\alpha} = \frac{\partial C_L}{\partial \alpha} = 2\pi \left(\frac{AR}{AR + 2} \right) \tag{4.38}$$

Moving on, the change in lift due to control surface deflection, Figure 4.7, can be described by Equation 4.39, with positive deflection being defined as down, positive z direction.

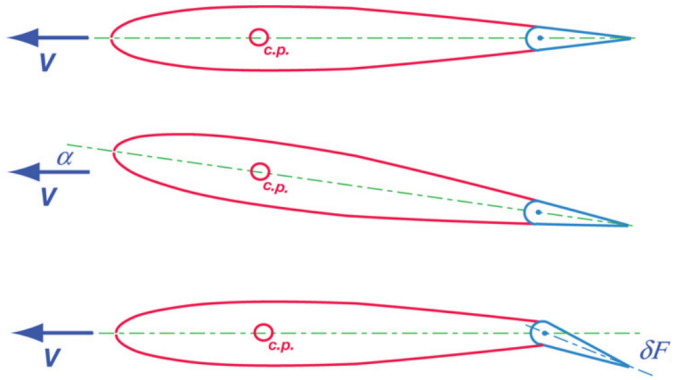

Figure 4.7. An Illustration of the Flaps deflection. Note that on the case UAV the Elevator is an all-moving tail [14]

$$C_{L_{\delta E}} = \frac{\partial C_L}{\partial \delta E} = \tau_{ht} \eta_{ht} (C_{L\alpha})_{ht} \frac{S_{ht}}{S} \tag{4.39}$$

Where τ_{ht} is the carryover effect from other deflections, which in the project case is neglected. The tail efficiency factor η_{ht} is set to 1 for the slow flying UAV. Alternatively,

for the horizontal tail, it can be replaced by a Sigmoid function for positive deflections, using $15(45^\circ - \alpha)$ as the exponent [14]. The subscript ht refers to the horizontal tail. This nomenclature of subscripting for partial derivatives will be retained for the remainder of the project.
The lift variation because of elevator deflection is then as in Equation 4.40.

$$\Delta Lift = C_{L_{\delta E}} \bar{q} S \delta E \tag{4.40}$$

The same principal structure also applies to deflection of the flaps, δF, as shown in Equation 4.41.

$$C_{L_{\delta F}} = (C_{L\alpha}) \frac{S_F}{S} \tag{4.41}$$

The horizontal tail lift is also sensitive to pitch rate, which can be described by Equation 4.42.

$$C_{L_{qht}} = \frac{\partial(\Delta C_{L_{ht}})_{ac}}{\partial q} = \left(\frac{\partial C_{L_{ht}}}{\partial \alpha} \right)_{ac} \frac{l_{ht}}{V} \tag{4.42}$$

where the subscript ac means it related to the aircraft reference area, S, and l_{ht} is the length from the center of mass for the aircraft to the horizontal tail center of pressure as shown in Figure 4.5.

Looking at drag, Equation 4.44 can be used to describe the total drag of the aircraft, and looks similar to the lift equation, except now the force direction is opposite the velocity vector instead of perpendicular as in the lift equation.

$$Drag = C_D \bar{q} S \tag{4.43}$$

$$C_D \approx C_{D_p} + C_{D_w} + C_{D_i} \approx C_{D_0} + \epsilon C_L^2 \tag{4.44}$$

With C_D being the drag coefficient, which can be split up in the contributing factors, C_{D_p}, C_{D_w} and C_{D_i} the parasitic, wave and the induced drag from lift, as shown in Equation 4.45. For the modelling of incompressible aerodynamics of this "slow" flying UAV the shock-wave induced drag is neglected.

$$C_{D_i} = C_L^2 / \ \pi \ e \ AR \tag{4.45}$$

Here e is the Oswald efficiency factor which is 1 for an elliptical lift distribution, which the case-UAV closely resembles. Equation 4.45 can be reduced by packaging constants as in Equation 4.46.

$$\epsilon = \frac{1}{\pi e AR} \tag{4.46}$$

With C_{D_w} neglected, thw zero-lift drag coefficient is equal to parasitic drag, which can be approximated as a base drag from the cross section of the fuselage and a flat-plate friction coefficient across the wetted area of the aircraft.

$$C_{D_0} = C_f \left(\frac{S_{wet}}{S} \right) + 0.12 \left(\frac{S_{base}}{S} \right) \tag{4.47}$$

where the friction coefficient C_f depends on the Reynolds number and therefore the air density, airspeed, and length of aircraft. To find the friction coefficient the Prandtl-Schlichting skin formula was used in this model.

As mentioned the solution for modeling in this project is to create tabulated calculations for each coefficient component with varying angles of attack. In simulation the current α is then used to interpolate the corresponding lift coefficient component. A total lift coefficient C_L is the sum of its components, as shown in Equation 4.48.

$$C_L = C_{L_{static}} + C_{L_q} q + C_{L_{\delta E}} E + C_{L_{\delta F}} F \tag{4.48}$$

At this point all components have been also been calculated in relation the the current angle of attack, so to get the body axis coefficients, Equations 4.49 and 4.50 are used.

$$C_X = -C_D \; cos\alpha + C_L \; sin\alpha \tag{4.49}$$

$$C_Z = -C_D \; sin\alpha - C_L \; cos\alpha \tag{4.50}$$

4.3.2 Pitching Moment

The pitching moment part of M_B or the moment about the y-axis is the pressure and shear stress differentials times the moment arms integrated across the surface of the aircraft. But it can be approximated as the sum of centers of pressure (cp) for the individual parts of the aircraft (fuselage, wing, tail, etc.) plus pure couples and interference effects.
Pure couples can be that for small angles of attack, the fuselage is expected to produce positive lift where the nose of the fuselage flairs out, and negative lift where the tail narrows. Potential interference effects are ignored for this modeling. The center of pressure will be assumed to the same as the aerodynamic center, which for symmetric wing profile can be approximated to be at $1/4\bar{c}$ of the wings. The pitching moment can be expressed as Equation 4.51, as shown in Section 4.1.3.

$$M_{B_y} = C_m \bar{q} S \bar{c} \tag{4.51}$$

Just as for the other non-dimensional aerodynamic coefficients, the pitching moment coefficient can also be separated into components, one of which is dependent on angle of attack.

$$M_{B_y} = (C_{m_0} + C_{m_\alpha}) \bar{q} S \bar{c} \tag{4.52}$$

Using C_{L_0}, C_{m_0} can be found through Equation 4.53.

$$C_{m_0} = -C_{L_0} SM \tag{4.53}$$

If C_m, as shown in Equation 4.52 inside the brackets, is seen as a line in the α-C_m-plane, then C_{m_0} is the crossing of the coefficient axis and the zero crossing will be the trim angle of attack. Also meaning that α_{trim} will be where the sum of the moments is zero.
For static stability, SM needs to be positive, or that the center of mass is in front of the center of pressure, and the $\partial C_m/\alpha$ slope should be negative as shown in Figures 4.8 and 4.9.

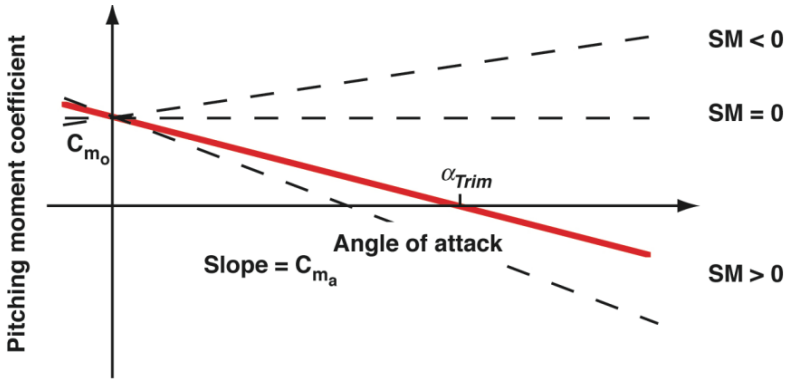

Figure 4.8. The α-C_m-plane [14]

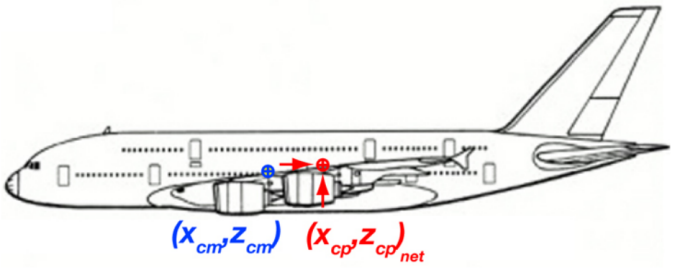

Figure 4.9. Illustration of center of mass and center of pressure [14]

Positive static margin in effect enables the nose to drop again if the aircraft is stalled and looses lift. Looking at Equation 4.52, α_{trim} can also be calculated as Equation 4.54.

$$\alpha_{trim} = -\frac{C_{m_0}}{C_{m_\alpha}} \tag{4.54}$$

For small α and no deflection of control surfaces C_{m_α} can be approximated as the normalised stability margin times the α dependent lift coefficient as shown in Equation 4.55, just like Equation 4.53.

$$C_{m_\alpha} = -C_{L_\alpha}(h_{cm} - h_{cp}) \tag{4.55}$$

For higher angles of attack the same procedure as for the lift and drag coefficients is used. As demonstrated for the lift coefficient, the pitching moment coefficient also shifts with control surface defection, as described by Equation 4.56.

$$M_{B_y} = (C_{m_0} + C_{m_\alpha} + C_{m_{\delta E}}\delta E)\bar{q}S\bar{c} \tag{4.56}$$

Having control surface deflections also changes Equation 4.54, as expected, to keep the sum of the moments zero. Deflections thereby allow the pitching moment to be negative, and force the nose down.

The pitching moment also changes with pitch rate, including $C_{m_q}q$ as a part of C_m.

$$\hat{q} = \frac{q\bar{c}}{2V} \tag{4.57}$$

$$C_{m_{\hat{q}}} = \frac{\partial C_m}{\partial \hat{q}} = \frac{\partial C_m}{\partial (q\bar{c}/2V)} = \left(\frac{2V}{\bar{c}}\right) C_{m_q} \Rightarrow$$

$$C_{m_q} = \left(\frac{\bar{c}}{2V}\right) C_{m_{\hat{q}}} \tag{4.58}$$

$$\frac{\partial M}{\partial q} = C_{m_q}(\rho V^2/2)S\bar{c} = C_{m_{\hat{q}}}\left(\frac{\bar{c}}{2V}\right)\left(\frac{\rho V^2}{2}\right)S\bar{c} \tag{4.59}$$

$$C_{m_{\hat{q}}} = -C_{m_{\hat{q}_{ht}}} - C_{m_{\hat{q}_{wing}}} = \left(-2C_{L_{\alpha_{ht}}}\left(\frac{l_{ht}}{\bar{c}}\right)^2\right) - (2C_{L_{\alpha_{wing}}}(SM - 0.75)^2) \tag{4.60}$$

Where $\hat{q}$ is the normalized pitch rate, not an estimate as the hat might suggest. This tail lift addition is the aerodynamic damping due to pitch rate.

Adding l_{ht} normalised with $\bar{c}$ to Equation 4.39, the pitching moment coefficient for Elevator deflection can be found, as Equation 4.61

$$C_{m_{\delta E}} = -\tau_{ht}\eta_{ht}(C_{L_\alpha})_{ht}\left(\frac{S_{ht}}{S}\frac{l_{ht}}{\bar{c}}\right) \tag{4.61}$$

Here τ_{ht} can be modeled as discussed along with Equation 4.39 and η_{ht} is ignored for the case mini-UAV. Downwash and elasticity effects could be included, but is ignored in this modeling.

4.4 Lateral forces

This section will describe the force and moment coefficents which govern movement out of the xz-plane.

4.4.1 Sideforces

When the aircraft sideslips a side force is induced, along with yawing and rolling moments.

The side force due to sideslip angle can be described by Equation 4.62.

$$Y \approx \frac{\partial C_Y}{\partial \beta}\bar{q}S\cdot\beta \tag{4.62}$$

Where, again, the aerodynamic coefficient can be separated in to components for different parts of the aircraft. The dominant components are those for the fuselage, wing and vertical tail, which can be described by Equations 4.63 to 4.66.

$$(C_{Y\beta})_{\text{Vertical tail}} \approx \frac{\pi AR_{vt}}{1 + \sqrt{1 + \left(\frac{0.5AR_{vt}}{cos\Lambda_{1/4vt}}\right)^2}}\left(\frac{S_{vt}}{S}\right) \tag{4.63}$$

$$(C_{Y\beta})_{Fuselage} \approx -2\frac{S_{Base}}{S} \tag{4.64}$$

$$(C_{Y\beta})_{Wing} \approx -C_{D_{0,Wing}} - k\Gamma^2, \qquad k = \frac{\pi AR}{1 + \sqrt{1 + AR^2}} \tag{4.65}$$

$$C_{Y\beta} = (C_{Y\beta})_{\text{Vertical tail}} + (C_{Y\beta})_{\text{Fuselage}} + (C_{Y\beta})_{\text{Wing}} \tag{4.66}$$

Where S_{base} is the cross-sectional area of the fuselage in the yz-plane, and Γ is the dihedral angle of the wings, as shown in Figure 4.5.

4.4.2 Yawing moment

The same form is applicable when it comes to the yawing moment as shown in Equation 4.67.

$$N \approx C_{n_\beta} \bar{q} S b \cdot \beta \tag{4.67}$$

Where the components of C_{n_β} are dominated by the vertical tail, fuselage, wing and propeller. For the vertical tail, Equation 4.68 can be used.

$$(C_{n_\beta})_{\text{Vertical tail}} \approx -C_{Y_{\beta_{vt}}} \frac{l_{vt}}{b} \tag{4.68}$$

Here l_{vt} is the distance from the aircraft center of mass to the vertical tail center of pressure, measured along the body x-axis, again shown in Figure 4.5. Notice that l_{vt} is normalised by the wingspan b.

Regarding the component from the fuselage, a simplified Equation using the stability margin, SM, can be expressed as in Eq. 4.69.

$$(C_{n_\beta})_{\text{Fuselage}} \approx 2 \frac{S_{base}\ SM}{S\ b} \tag{4.69}$$

And for the wing, a simplification can be written as Equation 4.70.

$$(C_{n_\beta})_{\text{Wing}} \approx 0.075 C_L \Gamma \tag{4.70}$$

4.4.3 Rolling moment

A rolling moment will be caused as a result of the unequal lift of the left and right wing, because of the flow direction during sideslip. Again the same format appears in Equation 4.71.

$$L \approx C_{l_\beta} \bar{q} S b \cdot \beta \tag{4.71}$$

Likewise C_{l_β} has components where the major contributors are from the wing, vertical tail and the vertical location of the wing on the fuselage, which causes up- and down-wash.

$$(C_{l_\beta})_{\text{Wing}} = -\frac{1+2\lambda}{6(1+\lambda)} \Gamma (C_{L_\alpha})_{Wing} \tag{4.72}$$

$$(C_{l_\beta})_{\text{Wing-Fuselage}} = 1.2\sqrt{\lambda}\ \frac{2 z_{wing} h_{fuselage}}{b^2} \tag{4.73}$$

$$(C_{l_\beta})_{\text{Vertical tail}} = -l_{vt} \frac{(C_{Y\beta})_{\text{vt}}}{b} \tag{4.74}$$

With z_{wing} and $h_{fuselage}$ being the placement of the wings on the fuselage and the maximum height of the fuselage. The wing taper ratio being denoted λ.

4.4.4 Lateral directional due to control surfaces

Sideforce coefficient also changes with rudder deflection as in Equation 4.77.

$$(C_{Y_{\delta R}})_S = [(C_{L_\alpha})_{vt}]_{S_{vt}} \ \tau_{vt}\eta_{vt}\frac{S_{vt}}{S} \tag{4.75}$$

$$\Delta C_Y = C_{Y_{\delta R}}\delta R \tag{4.76}$$

$$Y \approx (C_{Y_{\delta R}}\delta R + C_{Y\beta}\cdot\beta)\bar{q}S \tag{4.77}$$

As is the point, the yawing moment is changed with rudder deflections as shown in Equation 4.78.

$$C_{n_{\delta R}} = -\tau_{vt}\eta_{vt}(C_{L_\alpha})_{vt}\left(\frac{S_{ht}}{S}\frac{l_{ht}}{\bar{c}}\right) \tag{4.78}$$

Finally the Aileron deflection changes the rolling moment as shown in Equation 4.79, where the wingspan-aileronspan ratio, k_{wa}, is used.

$$C_{l_{\delta A}} \approx \frac{C_{L_a}}{1+\lambda}\left[\frac{1-k_{wa}^2}{3} \ - \ \frac{1-k_{wa}^3}{3}\ (1-\lambda)\right] \tag{4.79}$$

$$k_{wa} = \frac{y_A}{b/2} \tag{4.80}$$

Here y_A is the distance from center of mass to the inner edge of the ailerons. The carryover effect is neglected, as flaps and ailerons are the same surface.

Aerodynamic damping is also present for yaw- and roll-rate, as it was shown for pitch-rate in Equation 4.60.

$$\hat{p} = \frac{pb}{2V} \tag{4.81}$$

$$C_{l_p}(\rho V^2/2)Sb = C_{l_{\hat{p}}}\left(\frac{b}{2V}\right)\left(\frac{\rho V^2}{2}\right)Sb = C_{l_{\hat{p}}}\left(\frac{\rho V S b^2}{4}\right) \tag{4.82}$$

Looking at the roll damping, which should be negative for stability, and starting with the wings. For the case-UAV Equation 4.83 for tapered wings is used.

$$(C_{l_{\hat{p}}})_{Wing} = \frac{\partial(\Delta C_l)_{Wing}}{\partial\hat{p}} = \frac{C_{L_\alpha}}{12}\left(\frac{1+3\lambda}{1+\lambda}\right) \tag{4.83}$$

$$(C_{l_{\hat{p}}})_{vt} = -\frac{C_{Y_{\beta_{vt}}}}{12}\left(\frac{S_{vt}}{S}\right)\left(\frac{1+3\lambda}{1+\lambda}\right) \tag{4.84}$$

$$(C_{l_{\hat{p}}})_{ht} = -\frac{C_{L_{\alpha_{ht}}}}{12}\left(\frac{S_{ht}}{S}\right)\left(\frac{1+3\lambda}{1+\lambda}\right) \tag{4.85}$$

The same equation can be used for the vertical and horizontal wing, only referred to the wing area, in Equation 4.84 and 4.85.

Likewise the yaw damping can be expressed as Equation 4.89.

$$\hat{r} = \frac{rb}{2V} \tag{4.86}$$

$$C_{n_r}(\rho V^2/2)Sb = C_{n_{\hat{r}}}\left(\frac{\rho V S b^2}{4}\right) \tag{4.87}$$

$$(C_{n_{\hat{r}}})_{vt} = -2(C_{n_\beta})_{vt}\left(\frac{l_{vt}}{b}\right) \tag{4.88}$$

$$(C_{n_{\hat{r}}})_{Wing} = k_0 C_L^2 + k_1 C_{D_{0,wing}} \tag{4.89}$$

Where k_0 and k_1 are dependent on AR and sweep angle, for this project the values of -0.103 and -0.4 have been used, but this should be investigated further.

4.5 Aircraft Geometry

With the equations of motion and relevant non-dimensional aerodynamic equations defined, the necessary structural information about the aircraft can be tallied up. With some being relevant for several features of the aircraft, depending on the design.

- Total Mass m
- Center of mass cm
- Center of pressure cp
- Static margin SM
- Inertia matrix $\mathbf{I}$ - I_{xx}, I_{yy}, I_{zz}, I_{xz}
- Length l - ht, vt, fuselage
- Height h - fuselage
- Span b - wing, ht, vt, A, E, R
- Aspect Ratio AR - wing, vt, ht
- Mean aerodynamic chord $\bar{c}$ - wing, vt, ht, A, E, R
- Sweep angle Λ - wing, vt, ht
- Taper ratio λ - wing, vt, ht
- Dihedral angle Γ
- Area S - Wing, ht, vt, wetted, fuselage shadow, fuselage crosssection, propeller, ac.
- Maximum deflections δ_{max} - A, R, F
- Oswald efficiency factor e
- Flat plate friction coefficient cf
- Max static thrust T_{max}

From these, tables for the coefficients can be constructed for interpolation with angle of attack, sideslip angle, control deflection etc. Once each sub-component has been found, they can be summed to the overall coefficients as introduced in Equations 4.1 and 4.2.

$$C_L = C_{L_{static}} + C_{L_q} q + C_{L_{\delta E}} \delta E + C_{L_{\delta F}} \delta F \tag{4.90}$$

$$C_D = C_{D_0} + \epsilon C_L^2 + C_{D_q} q + C_{D_{\delta E}} \delta E + C_{D_{\delta F}} \delta F \tag{4.91}$$

$$C_m = C_{m_{static}} - C_L SM + C_{m_q} q + C_{m_{\delta E}} \delta E + C_{m_{\delta F}} \delta F \tag{4.92}$$

$$C_Y = C_{Y_\beta} \beta + C_{Y_p} p + C_{Y_r} r + C_{Y_{\delta A}} \delta A + C_{Y_{\delta R}} \delta R \tag{4.93}$$

$$C_l = C_{l_\beta} \beta + C_{l_p} p + C_{l_r} r + C_{l_{\delta A}} \delta A + C_{Y_{\delta R}} \delta R \tag{4.94}$$

$$C_n = C_{n_\beta} \beta + C_{n_p} p + C_{n_r} r + C_{n_{\delta A}} \delta A + C_{n_{\delta R}} \delta R \tag{4.95}$$

Where C_X and C_Z are found as described in Equations 4.49 and 4.50, and then applying the Equations of motion.

4.6 Trim flight

With the governing equations defined, the trim flight conditions can also be calculated. Continuing from the Equations in Section 4.3.1. From a purely longitudinal viewpoint, the velocity magnitude and flight path angle can be derived from the inertial frame velocity in the x and z direction, as in Equation 4.96.

$$\begin{bmatrix}\dot{x}\\ \dot{z}\end{bmatrix} = \begin{bmatrix}v_x\\ v_z\end{bmatrix} = \begin{bmatrix}V\cos\gamma\\ -V\sin\gamma\end{bmatrix} \Rightarrow \begin{bmatrix}V\\ \gamma\end{bmatrix} = \begin{bmatrix}\sqrt{\dot{x}^2+\dot{z}^2}\\ -sin^{-1}(\frac{\dot{z}}{V})\end{bmatrix} = \begin{bmatrix}\sqrt{v_x^2+v_z^2}\\ -sin^{-1}(\frac{v_z}{V})\end{bmatrix} \tag{4.96}$$

Considering the aircraft as a point mass, the state transition equation for V and γ can be expressed as Equations 4.5, except with respect to γ instead of θ. The angle of attack is considered, as the thrust coefficient is used with thrust being aligned with the aircraft x-axis

$$\dot{V} = \frac{(C_T\cos\alpha - C_D)\frac{1}{2}\rho(z)V^2S - mg_o\sin\gamma}{m} \tag{4.97}$$

$$\dot{\gamma} = \frac{(C_T\sin\alpha + C_L)\frac{1}{2}\rho(z)V^2S - mg_o\cos\gamma}{mV} \tag{4.98}$$

To aid the reader, Figure 4.3 is repeated below.

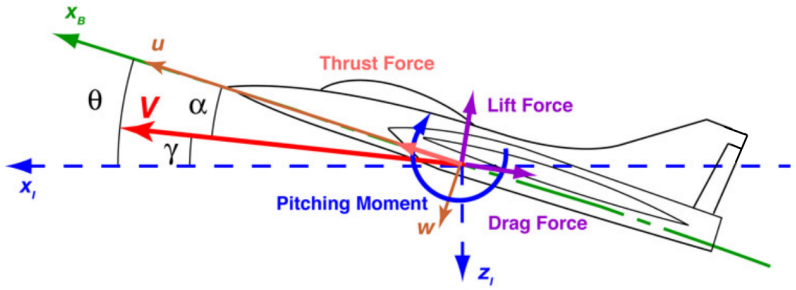

Figure 4.10. Longitudinal variables [14]

Then for steady level flight, $\alpha \sim 0$ and $v_z = 0$. So $\dot{V} = 0$ and $\gamma = 0$ as the velocity vector is aligned with the inertial x-direction.

$$\dot{V} = 0 = \frac{(C_T - C_D)\frac{1}{2}\rho(z)V_{cruise}^2S}{m} \tag{4.99}$$

$$\dot{\gamma} = 0 = \frac{C_L\frac{1}{2}\rho(z)V_{cruise}^2S - mg_o}{mV_{cruise}} \tag{4.100}$$

Equations 4.99 and 4.100 basically says that thrust is equal to drag and lift is equal to weight of the aircraft, so the altitude is constant and the airspeed is constant.

Then the most efficient conditions under which to stay in steady level flight is where drag is at its lowest while still maintaining sufficient lift. As parasitic drag increases with V exponentially and lift induced drag has the inverse relation, the global minimum drag corresponds to a certain airspeed, as shown in Figure 4.11.

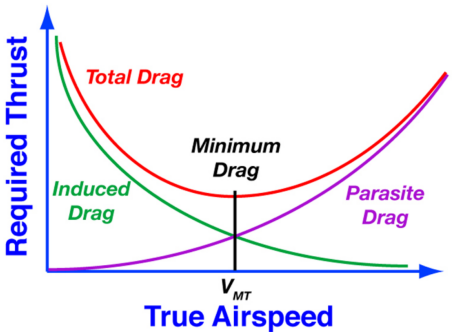

Figure 4.11. Contribution of drag components [14]

The maximum lift to drag ratio can be found through choosing C_L. Since both lift and drag is expressed with the same reference area and dynamic pressure, the ratio can be written as Equation 4.101

$$\frac{L}{D} = \frac{C_L}{C_D} = \frac{C_L}{C_{D_0} + \epsilon C_L^2} \tag{4.101}$$

Then the zero slope point can be found as in Equation 4.102.

$$\frac{\partial(L/D)}{\partial C_L} = 0 = \frac{(C_{D_0} + \epsilon C_L^2) - C_L(2\epsilon C_L)}{(C_{D_0} + \epsilon C_L^2)^2} = \frac{(C_{D_0} - \epsilon C_L^2)}{(C_{D_0} - \epsilon C_L^2)^2} \tag{4.102}$$

And the lift coefficient should be as in Equation 4.103.

$$(C_L)_{(L/D)_{max}} = \sqrt{\frac{C_{D_0}}{\epsilon}} \tag{4.103}$$

$$(L/D)_{max} = \frac{1}{2\sqrt{\epsilon C_{D_0}}} \tag{4.104}$$

The required lift is opposite the weight of the aircraft, to keep the force balance and level flight, as seen in Equation 4.105.

$$\begin{aligned} W &= C_{L_{trim}} \bar{q} S \\ C_{L_{trim}} &= \frac{1}{\bar{q}}(W/S) = \left(\frac{2e^{\beta h}}{\rho_0 V^2}\right)(W/S) \end{aligned} \tag{4.105}$$

Where $C_{L_{trim}}$ can be written with the dynamic pressure as a function of altitude as discussed in Equation 4.22. The trim angle of attack can be expressed as Equation 4.106

$$\alpha_{trim} = \frac{\frac{1}{\bar{q}}(W/S) - C_{L_0}}{C_{L_\alpha}} \tag{4.106}$$

Where W/S is the wing loading.

This can also be seen from the following derivation. The thrust required is equal to the sum of parasitic and induced drag, as shown in Equation 4.107.

$$T_{trim} = D_{cruise} = C_{D_0} \bar{q} S + \epsilon \frac{2W^2}{\rho V^2 S} \tag{4.107}$$

$$\frac{\partial T_{trim}}{\partial V} = C_{D_0}(\rho V S) - \frac{4\epsilon W^2}{\rho V^3 S} = 0 \tag{4.108}$$

While in Equation 4.108, the necessary condition of zero slope is shown. This can also be put differently as in Equation 4.109.

$$C_{D_0}(\rho V S) = \frac{4\epsilon W^2}{\rho V^3 S} \tag{4.109}$$

$$\frac{\partial^2 T_{trim}}{\partial^2 V} = C_{D_0}(\rho S) + \frac{12\epsilon W^2}{\rho V^4 S} > 0 \tag{4.110}$$

Also the curvature should be positive as shown in Equation 4.110.

For the minimum airspeed, Equation 4.111 can be expressed as a rearrangement of Equation 4.108.

$$V^4 = \frac{4\epsilon}{C_{D_0}\rho^2}(W/S)^2 \Rightarrow$$

$$V_{\text{min.T}} = \sqrt{\frac{2}{\rho}\left(\frac{W}{S}\right)\sqrt{\frac{\epsilon}{C_{D_0}}}} \tag{4.111}$$

The solution, the velocity that requires the least thrust, is the the positive root of Equation 4.111. Knowing the minimum-thrust velocity, the lift coefficient can be found by Equation 4.112

$$C_{L_{\text{min.T}}} = \frac{2}{\rho V_{\text{min.T}}^2}\left(\frac{W}{S}\right) = \sqrt{\frac{C_{D_0}}{\epsilon}} = (C_L)_{(L/D)_{max}} \tag{4.112}$$

With Equation 4.112 arriving at the same conclusion as Equation 4.103

If a certain airspeed is required a minimization algorithm can be used for the equations of motion, specifically the velocity change in x and z directions,x_1 and x_3, and the pitch rate x_8.

System Identification 5

In this chapter the utilization of System IDentification Program for AirCrafts, SIDPAC, is presented as another option for increasing accuracy of an aircraft model.

5.1 SIDPAC

Aircraft system identification is in short a mathematical modelling of an aircraft based on imperfect experimental data. System identification is also called the invers problem, as normally the task is to do simulation or control. In simulation the plant model and input is given, and output is found. For control the plant and output is given, and input shaping is designed. But for identification the inputs and outputs are given, and the plant model is to be found. For this problem SIDPAC, among other software or techniques can be used.

SIDPAC is a collection ∼350 of matlab scripts developed and tested by NASA Langley Research Center, specifically Dr. Eugene A. Morelli and Dr. Vladislav Klein. It has been used on a wide variety of aircrafts including the Global Hawk, Ares 1-x, X43A, twin otter and subscale aircrafts. So covering everything from UAVs, spaceflight launch systems and propeller crafts to hypersonic flight.

The problem of aircraft system identification is the same as from the start of Chapter 4. In the aerodynamic model assembly, some unknown parameters are required for defining the forces and moments from Newtons second law. Specifically the aerodynamic forces should be found as a function of quantities that can be measured, such as the inputs to the control surfaces or IMU measurements (states).

As aircraft system identification is based on data from a full-scale aircraft it is considered a more accurate method, compared to the analytical approach, CFD or wind-tunnel testing of a smaller scale the aircrafts.

There are two common options for system identification, equation error or output error solutions. For the equation error method, the forces and moments are isolated in the equations of motion, and the states are measured or calculated, as the example shown in Equation 5.2.

$$\dot{q} = \frac{M - (I_{xx} - I_{zz})pr - I_{xz}(p^2 - r^2)}{I_{yy}} \Rightarrow \tag{5.1}$$

$$M = I_{yy}\dot{q} + (I_{xx} - I_{zz})pr + I_{xz}(p^2 - r^2) \tag{5.2}$$

Data can then be used to calculate the forces and moments. A model structure, as Equation

5.3, is then proposed to explain those forces and moments as a functions of stats or inputs.

$$\hat{M} = M_0 + M_\alpha \alpha + M_q q + M_{\delta E} \delta E \tag{5.3}$$

The unknown parameters are then estimated by minimizing the error between the calculated forces or moments and the forces or moments from the proposed model. This is done using the least squares method, Equation 5.4

$$J = \frac{1}{2}(M - \hat{M})^T (M - \hat{M}) \tag{5.4}$$

For the output error method, the equations of motion are used as they are in Equations 4.5-4.17. The proposed model is the substituted in to the equations of motion and numerically integrated. The parameters are estimated to minimize the error between the output of the modeled state or output and the measured state/output, in the example above that would be q. Again using the least squares method.

The results from a system identification should be both the values and uncertainties of the unknown parameters.

For an aircraft in flight, the forces and moments can not be measured directly and large datasets with measurement noise are to be processed.

5.2 Data Pre-processing

The control and measurements on the case UAV are as many others done by an open-source flight control. The recorded flight data is stored as ulog files which can easly viewed a variety of software and matlabs "flight log analyser" app. Unfortunately SIDPAC can not easily read the ulog files. Therefore a seperate matlab script was made to quicker load, index, downsample, convert and restructure data series to be accepted by SIDPAC.

The data format for SIDPAC is a matrix with a column for each parameter as shown in Appendix A. The vectors of measurement have to be of the same length and sampling time, but as the flight control and the sensors have different sampling times, the above mentioned downsampling is required. Likewise, the unit of the measurements have to be converted to imperial units before opening SIDPAC, to avoid manual conversion for each new system identification. The pre-processing psudo-code is shown below.

- Load the ulog file - ulogreader(path)
- Choose start time and duration
- Read messages from the topics of interest for the time segment chosen - readtopicmsgs(file, topic, time)
- Individually index and properly name the topic channel data
- Downsample or upsample data vectors to fit the time vector - downsample(data, ratio), upsample() or imresize()
- Conversion to imperial units
- Data assembly in the "fdata"- matrix

SIDPAC also needs a reference area, inertia matrix, wingspan and chord length.

5.3 System identification

The SIDPAC UI is illustrated in Figure 5.1, with a plot of the highlighted data series.

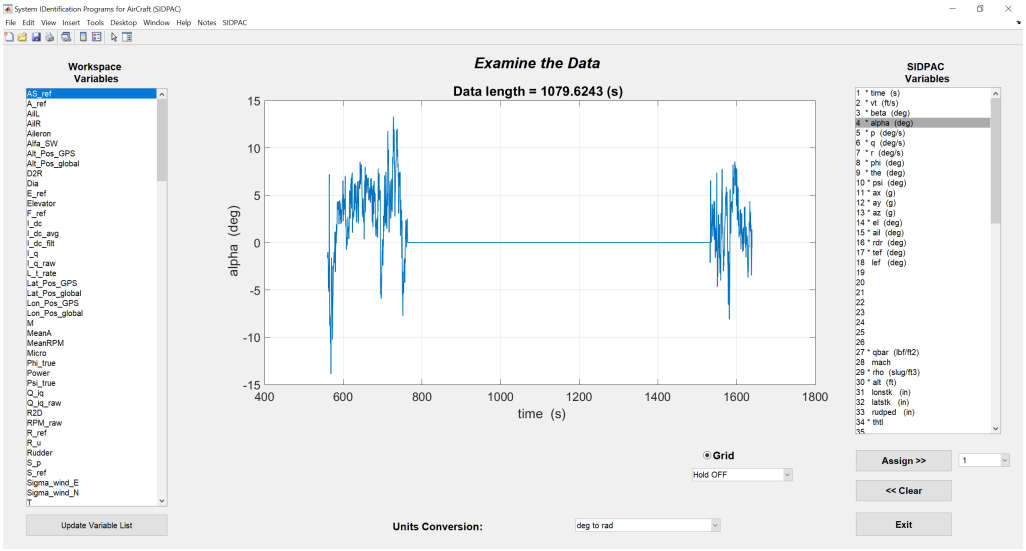

Figure 5.1. SIDPAC UI, with a corrupted α measurement shown

The * indicates that SIDPAC has accepted the data vector. For identification a segment or maneuver of the data set is cut out as shown in Figure 5.2.

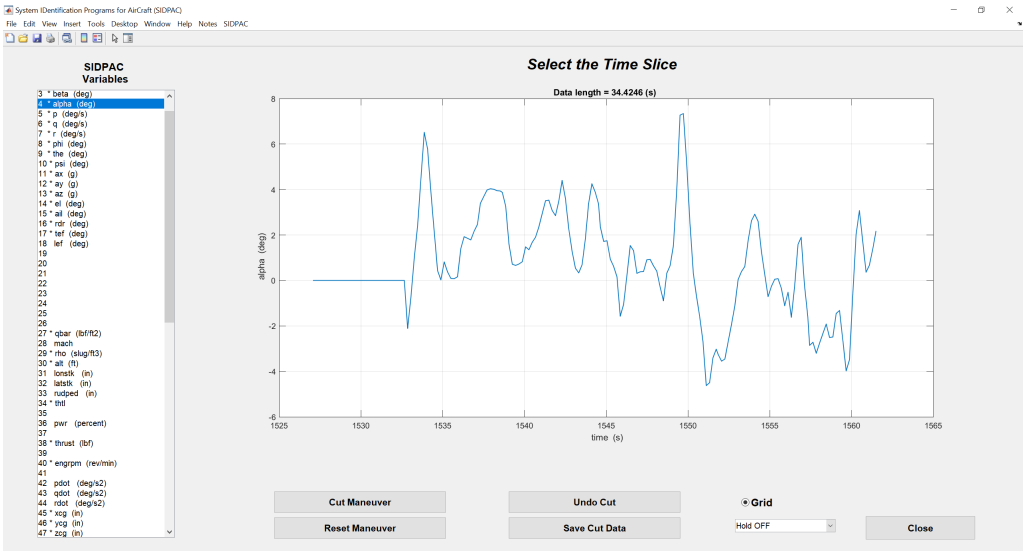

Figure 5.2. The SIDPAC cut maneuver UI

For this project the data cut is processed with the step-wise regression option. Here the equation error method is used, as discussed. Choosing either lateral or longitudinal dynamics the non-dimensional aerodynamic coefficients, C_X, C_Y, C_Z, C_l, C_m, and C_n can be estimated one at a time, illustrated in Figure 5.3.

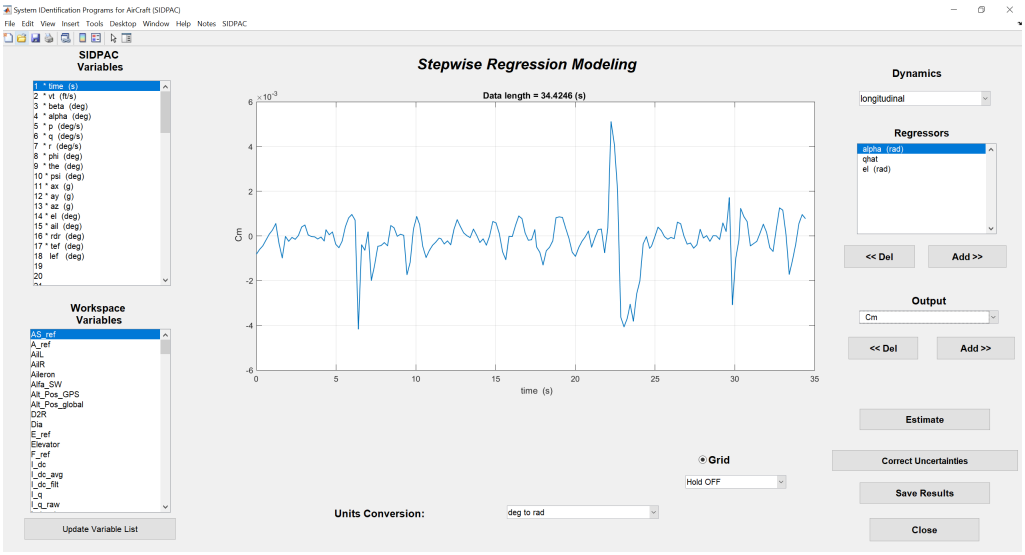

Figure 5.3. The SIDPAC stepwise regression UI

After estimation, the terms can be toggled in and out, while observing the model fit as shown in Figure 5.4, and saving when satisfied.

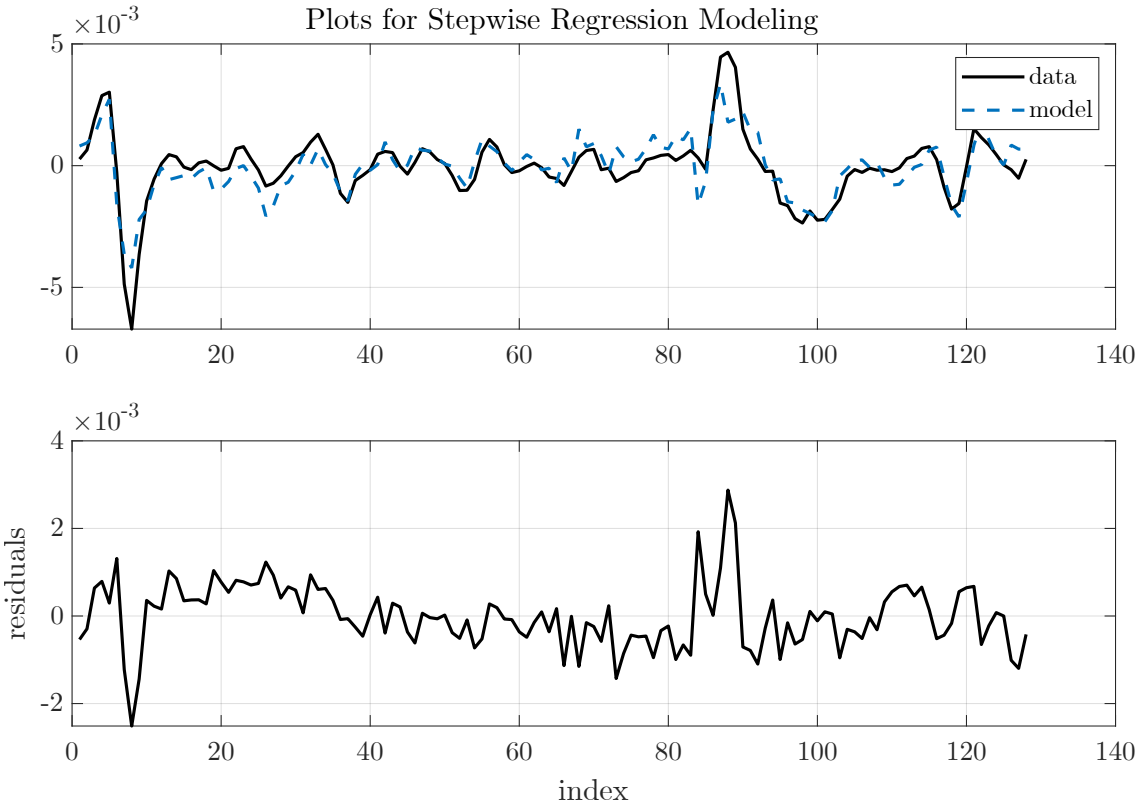

Figure 5.4. The fit of C_m to data. Non-dimensional on the y axis, and seconds on the x-axis

In Figure 5.4 the pitching moment coefficient is fitted to a segment of the flight data which showed some excitation in the xz-plane. In the code, C_m is calculated as Equation 5.5, as

expected from Equations 4.1 and 5.2.

$$C_m = (I_{yy}\dot{q} + I_{xz}(p^2 - r^2) + (I_{xx} - I_{zz})pr)/(\bar{c}\bar{q}S) \tag{5.5}$$

The regressors where α, $\hat{q}$, δE and throttle command. Also β, θ and δF where included because of the UAVs size, and that the influence could have been substantial. For the system identification, the model fit was between 24.5 and 88.9% but suitable data segment with minimal simultaneous actuation was not easily found. In Figure 5.5 an example of the output is shown, this time for C_X.

```
y = p(1)*x1 + p(2)*x2 + p(3)*x3 + p(4)*x4 + p(5)*x5 + p(6)*x6 + p(7)*x7 + p(8)

Parameter     Estimate    Std Error   % Error   95 % Confidence Interval     Index
---------     --------    ---------   -------   ------------------------     -----
 p( 1 )      1.857e+01    7.778e+00     41.9    [    3.015 ,   34.127 ]      1
 p( 2 )      4.281e+03    4.661e+02     10.9    [ 3348.675 , 5213.247 ]      10
 p( 3 )     -3.200e+02    3.607e+01     11.3    [ -392.134 , -247.865 ]      100
 p( 4 )      1.087e+00    1.972e-01     18.2    [    0.692 ,    1.481 ]      1000
 p( 5 )     -1.749e+01    3.057e+00     17.5    [  -23.601 ,  -11.371 ]      10000
 p( 6 )     -4.430e-01    2.429e-02      5.5    [   -0.492 ,   -0.394 ]      100000
 p( 7 )     -4.923e-01    8.546e-02     17.4    [   -0.663 ,   -0.321 ]      1000000
 p( 8 )     -1.530e+01    2.840e+00     18.6    [  -20.980 ,   -9.620 ]      0


x1 =   alpha  (rad)
x2 =   qhat
x3 =   el  (rad)
x4 =   tef  (deg)
x5 =   beta  (deg)
x6 =   thtl
x7 =   the  (deg)
x8 =   bias
```

Figure 5.5. Output of Stepwise regression for C_X

As with the first model, all the direct measured results will not be shown, to avoid business disruption.

For accurate system identification, the system excitation should have been done with uncorrelated actuator input, so as to be able to separate the input/output relations. The data used for this system identification is however not optimised for system identification, as the flights where done with a separate purpose.

Also wind disturbance is expected to be of relatively large magnitude for a mini-UAV compared to a manned aircraft with significantly more thrust. Therefore, a perfect fit can not be expected.
To be most effective, a pre-designed input should be introduces directly as an addition to the actuation signals, unaltered by any control loop [7].
To ensure excitation, different actuation frequencies should be used. Also to avoid correlation each actuator can sequentially be given an input which is a harmonic of the sampling rate. It can be proven that these sinusoidals are orthogonal and therefore uncorrelated [12]. The inputs should however be phase shifted to avoid unnecessary constructive interference and large amplitude inputs [7].

When the system identification process is set up, the approach is useful for R&D as new models can quickly be identified when modification are made to the aircraft, which is vital for control law design and simulation.

TAS Estimation 6

To increase the accuracy of navigation a key factor is information about the airspeed. As shown in both modelling approaches the forces and moments are proportional to the dynamic pressure, and therefore airspeed. When GNSS is not available, the only source of speed measurement is the accelerometer, which could cause the "simulation" to drift from the true speed.

In Section 2.4 is was also discussed that addition of pitot-tubes are not the first choice. However there might be another option, using the incoming air to propeller and BLDC.

6.1 FOC

It can be shown that for some BLDC designs and winding configurations, the use of field oriented control, FOC, is an efficient alternative to trapezoidal control [1]. In this context a BLDC is defined as having concentrated windings, but not necessarily produce a trapezoidal BEMF. Besides catering to distinct BEMF shapes, a difference between trapezoidal control and the FOC algorithm is that the latter requires information about the electric machine it is running. The point is that for commercial UAVs, prior knowledge about the motor construction is a given, therefore the plug-and-play advantage of trapezoidal control is less relevant. The advantage of FOC is that it introduces new states, measurements and control options. Specifically the rotor speed and the dq-currents are of interest. In the case-UAV the BLDC is a 12N14P out-runner motor, which means the stator has 12 poles and the rotor has 14 permanent magnets inside the bell. The BLDC windings are in a dLRK configuration, illustrated in Figure 6.1, which is a delta connected.

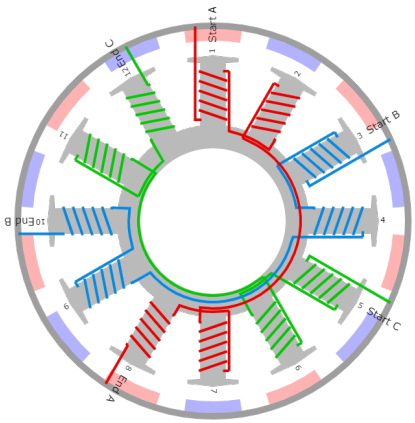

Figure 6.1. The winding scheme, with sequence AabBCcaABbcC, having the same phase for two consecutive tabs, with alternating polarity

In the case-UAV, the observed BEMF when measuring between two phases, and spinning the rotor, is nearly sinusoidal. Through the use of a thrust-stand laboratory setup, the efficiency of both control algorithms where compared, as shown in Figure 6.2.

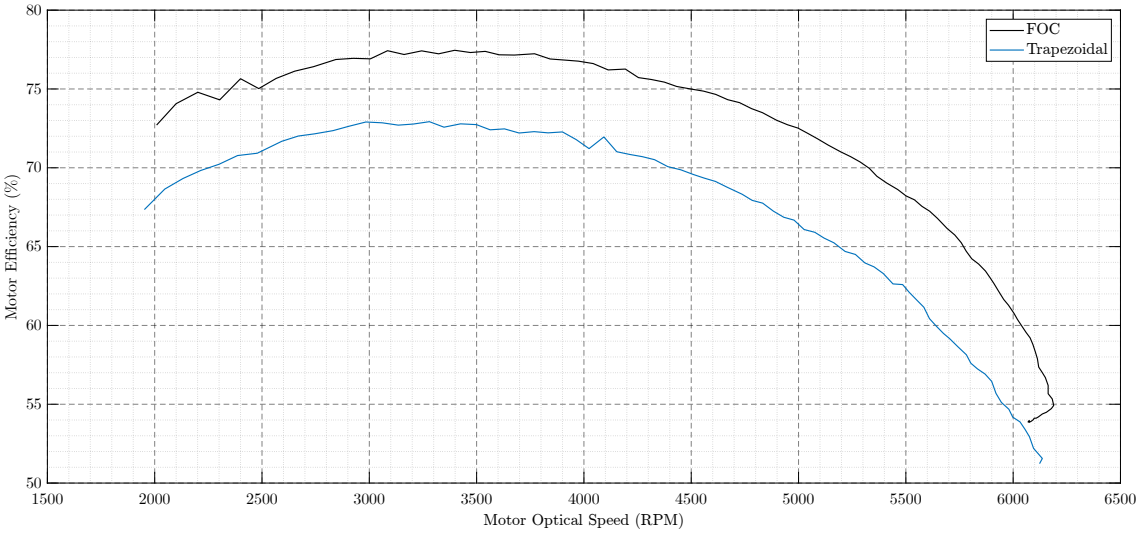

Figure 6.2. RPM-ramp test comparison of FOC and Trapezoidal control, for the specific model of 12N14P delta connected motor, using a Tyto-robotics 1585 thrust-stand

As can be seen in Figure 6.2, FOC is a more efficient control algorithm for the case-UAV.

The BLDC can be modeled as in Equation 6.1.

$$J\dot{\omega}_r = K_\tau i_q - B_v\omega_r - Q_L \tag{6.1}$$

Where Q_L it the load torque, which is governed by the propeller aerodynamics, ω_r is the mechanical rotor speed and B_v is the viscous friction. K_τ is the torque constant that relates the motor torque to the q-axis current. Lastly J is the inertia of the rotor, and what ever is mounted to it, combined. Here the near linear relation between i_q and torque Q can be used as measure of the mechanical torque if viscous friction is ignored.

It will now be assumed that the motor torque is equal and opposite the load torque for steady state conditions, and that the load torque is dominated by the torque from the propeller.

Knowing the rotor speed and propeller torque from the FOC algorithm, the governeing equations for propeller aerodynamics and experimental tabulated data is used in an attempt to "measure" the free-stream airspeed, TAS, from the q current and sensorless rotor speed estimate.
The q current is found through the abc-current and voltage sensors already in the case UAV. The measured parameters, in this case abc-current, is transformed from abc to $\alpha\beta$ an then to the $dq0$-frame using the Clark and Park transforms combined in Equations 6.2 and 6.3.

$$\mathbf{f}_{dq0} = \begin{bmatrix} f_d \\ f_q \\ f_0 \end{bmatrix} = \frac{2}{3}\begin{bmatrix} \cos(\theta_e) & \cos\left(\theta_e - \frac{2\pi}{3}\right) & \cos\left(\theta_e + \frac{2\pi}{3}\right) \\ -\sin(\theta_e) & -\sin\left(\theta_e - \frac{2\pi}{3}\right) & -\sin\left(\theta_e + \frac{2\pi}{3}\right) \\ \frac{1}{2} & \frac{1}{2} & \frac{1}{2} \end{bmatrix}\begin{bmatrix} f_a \\ f_b \\ f_c \end{bmatrix} \tag{6.2}$$

$$\mathbf{f}_{abc} = \begin{bmatrix} f_a \\ f_b \\ f_c \end{bmatrix} = \begin{bmatrix} \cos(\theta_e) & -\sin(\theta_e) & 1 \\ \cos\left(\theta_e - \frac{2\pi}{3}\right) & -\sin\left(\theta_e - \frac{2\pi}{3}\right) & 1 \\ \cos\left(\theta_e + \frac{2\pi}{3}\right) & -\sin\left(\theta_e + \frac{2\pi}{3}\right) & 1 \end{bmatrix} \begin{bmatrix} f_d \\ f_q \\ f_0 \end{bmatrix} \tag{6.3}$$

Here θ_e is the angle between the stator phase a flux axis and the d-axis.

The voltage and flux linkage for the BLDC in dq-frame are as shown below in Equations 6.4 to 6.7.

$$u_q(t) = R_s i_q(t) + \dot{\lambda}_q(t) + \omega_e(t)\lambda_d(t) \tag{6.4}$$
$$u_d(t) = R_s i_d(t) + \dot{\lambda}_d(t) - \omega_e(t)\lambda_q(t) \tag{6.5}$$
$$\lambda_q(t) = L_q i_q(t) \tag{6.6}$$
$$\lambda_d(t) = L_d i_d(t) + \lambda_{mpm} \tag{6.7}$$

u is the voltage, R_s is the phase resistance, λ_d and λ_q are the flux linkages. The BLDC can be considered to be close to non-salient, which simplifies the torque Equation 6.8 to Equation 6.9.

$$Q(t) = \frac{3}{2} n_{pp}(\lambda_d i_q(t) - \lambda_q i_d(t)) \Rightarrow$$
$$Q(t) = \frac{3}{2} n_{pp}\Big[\lambda_{mpm} i_q(t) + (L_d - L_q) i_d(t) i_q(t)\Big] \tag{6.8}$$
$$Q(t) = \frac{3}{2} n_{pp} \lambda_{mpm} i_q = K_\tau i_q(t) \tag{6.9}$$

Here n_{pp} is the number of pole pairs and λ_{mpm} is the peak rotor flux linkage. Lastly $L_q - L_d$ is the difference in inductance between the q and d axis, which is approximately zero (non-salient).

Having established the relation between measured current and torque, the load can be addressed.

6.2 Governing propeller equations

The governing equations for a propeller are shown in Equation 6.10 to 6.15[5].

$$\eta_{prop} = \frac{TV}{P_{mech}}, \qquad \eta_{prop} = \frac{C_T J}{C_P} \tag{6.10}$$

$$\tag{6.11}$$

$$J = \frac{V}{nd}, \qquad P_{mech} = Qn2\pi \tag{6.12}$$

$$\tag{6.13}$$

$$C_T = \frac{T}{\rho n^2 d^4}, \qquad C_P = \frac{P_{mech}}{\rho n^3 d^5} \tag{6.14}$$

$$\tag{6.15}$$

Here n is revolutions pr second and d is the diameter of the propeller. One way to calculate the propeller efficiency is the ratio between power input and work done, as shown in Equation 6.10. Where T is Thrust, V is the airspeed of the UAV while P_{mech} is the mechanical power applied by the rotor-shaft [9].
But the efficiency of propellers are often expressed by advance ratio, J together with the thrust and power coefficients, C_T and C_P, as shown in Equation 6.11. In this case the reference area of the thrust coefficient is usually the surface area of the propeller. Both C_T and C_P are functions of air density which is covered in Equation 4.22. More importantly, the torque coefficient for the propeller, C_Q, can be found through a simple relation with the power coefficient.

$$C_Q = \frac{C_P}{2\pi} \tag{6.16}$$

$$C_Q = \frac{Q}{\rho n^2 d^5} \tag{6.17}$$

Like many propellers the case-UAV propeller has been characterised through wind tunnel testing, and as such the power and thrust coefficient in relation to both efficiency and advance rate is tabulated in a database as shown in Figure 6.3.

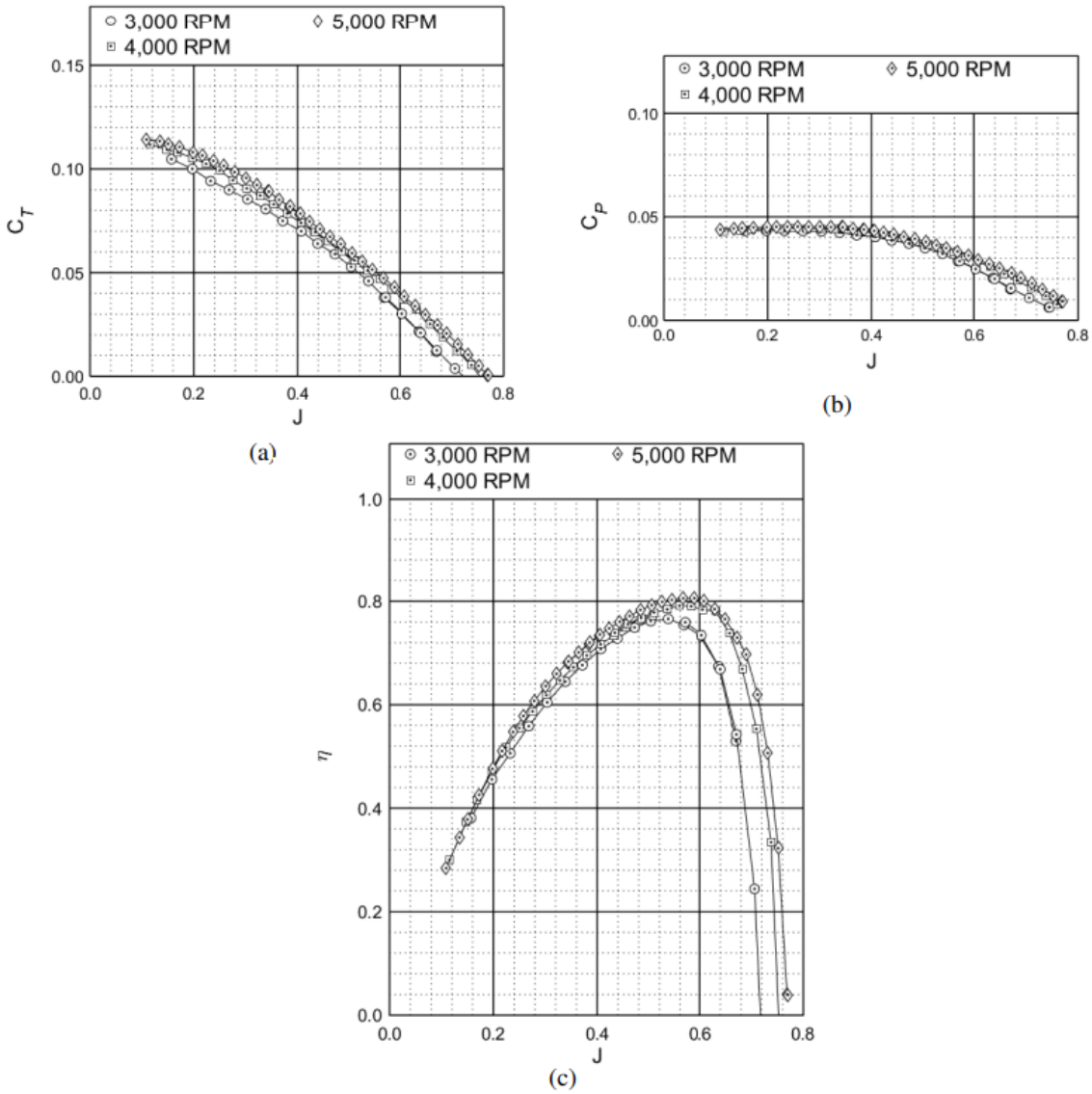

Figure 6.3. Eta, C_T and C_P with advance rate from the UIUC database [2]

In Figure 6.3(c) the same pattern as stall for high angle of attack is visible. The advance ratio is an important factor in efficient operation of a propeller. The stall problem is why variable pitch propellers are used, to efficiently accommodate different air speeds [5]. With that, the governing equations for a propeller and the torque equation for the BLDC can be combined through tabulated data to form a relation between i_q and V.

$$Q = K_t i_q = C_Q \rho n^2 d^5 \quad \Rightarrow \quad C_P = 2\pi \; C_Q = 2\pi \; \frac{K_t i_q}{\rho n^2 d^5} \tag{6.18}$$

In Equation 6.18, K_t and d are constants, and both ρ, n and i_q are measured either by the flight controller or FOC, C_Q can be isolated and used to find the advance ratio through the tabulated relation with C_P.

$$J = LUT(C_P) \tag{6.19}$$

$$V = JnD \tag{6.20}$$

In Equation 6.20 the final step from advance rate to airspeed through a LookUpTable is shown.

6.3 Implementation

As the stepsize of tested propeller speeds in the database are somewhat large, a polynomial fit of the tabulated data was made instead of an interpolation.

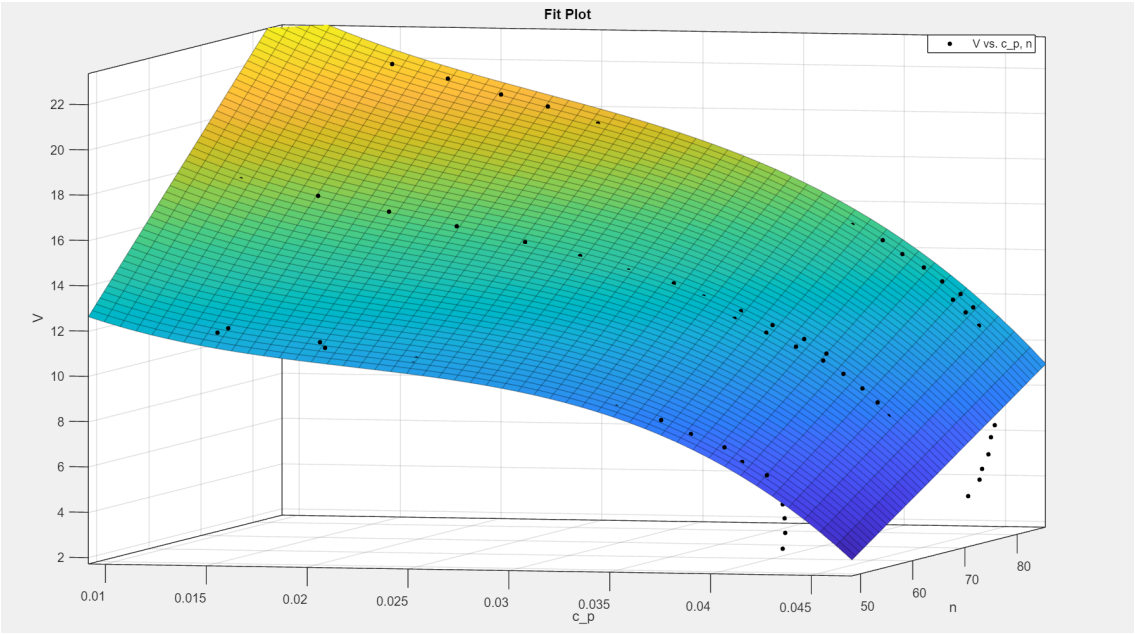

Figure 6.4. Plot of the poly-fit made with matlab curvefit tool

From Figure 6.4 it can be seen the third order polynomial captures the "lift slope" adequately but does not represent the post-stall data effectively. This is accepted to keep the polynomial of a lower order, for this proof of concept, as post-stall is not the desired state of operation. The fit has an R-squared value of 0.96, which is deemed sufficient for now. Implementing the polynomial as a substitute for the LUT, an estimate of airspeed can be calculated from real flight data. In this example, the case UAV flies in circles as shown in Figure 6.5, with the red dot indicating the start and the blue end of flight.

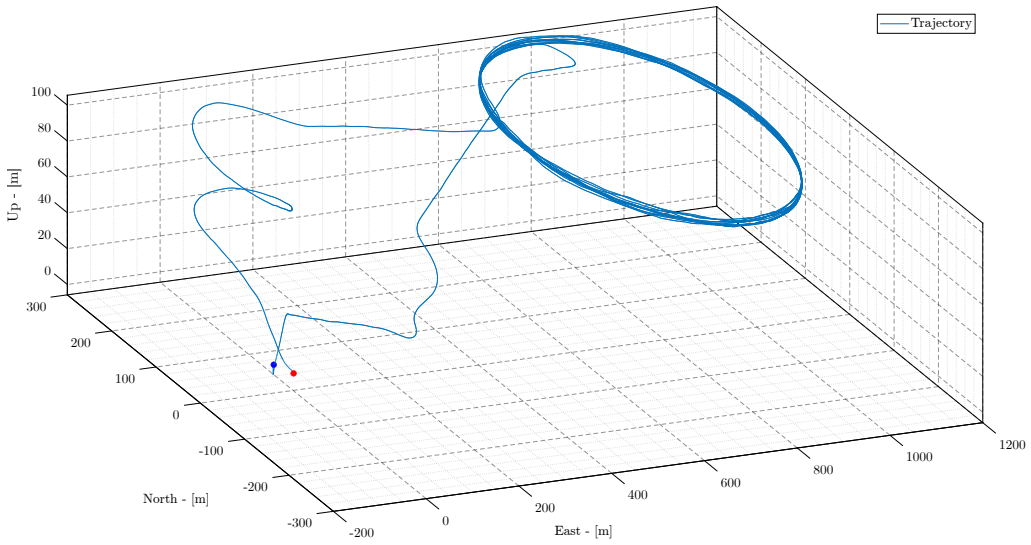

Figure 6.5. Estimated True Air Speed from FOC states i_q and n and the inertial reference frame velocity magnitude from GPS

The airspeed estimate is plotted along the GPS measured velocity magnitude, in Figure 6.6.

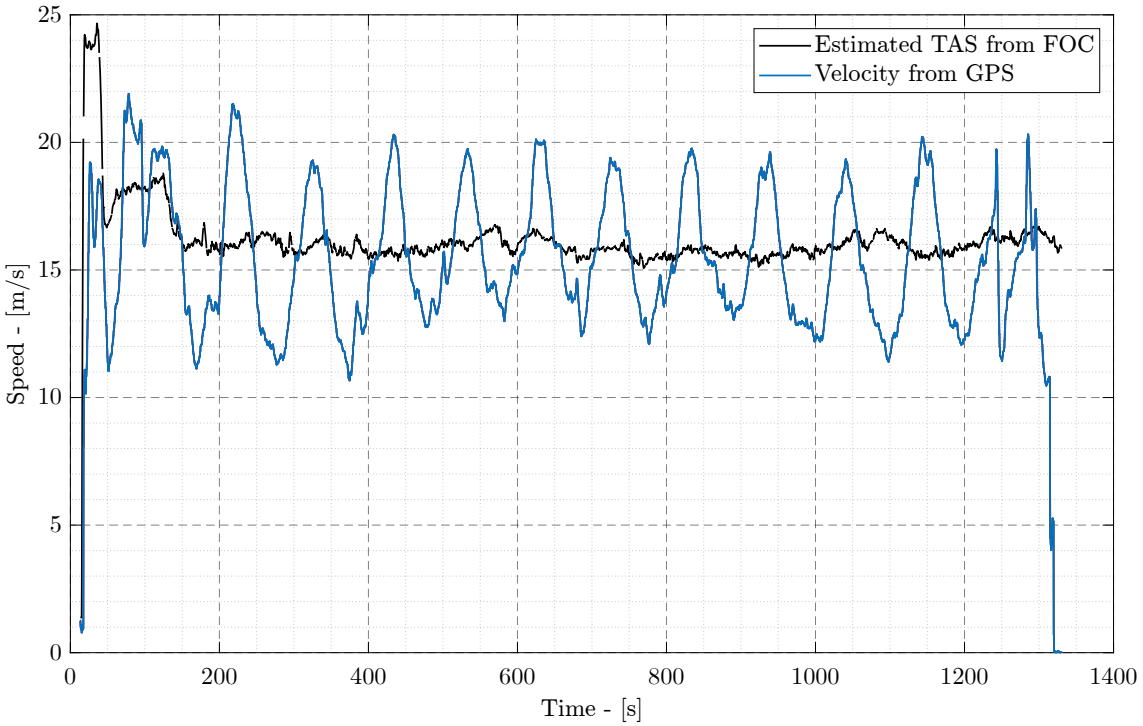

Figure 6.6. Estimated True Air Speed from FOC states i_q and n and the inertial reference frame velocity magnitude from GPS

The GPS velocity oscillates in magnitude as the case-UAV experiences varying wind due to the circular flight path. From DMI weather archives the wind was 2.4-3.1 m/s mean wind from north-north-west and turning north-west towards the end of the flight. Gusts where 5.2-6.3 m/s. If plotted along with the yaw estimate form the flight log, the correlation seams valid, shown in Figure 6.7.

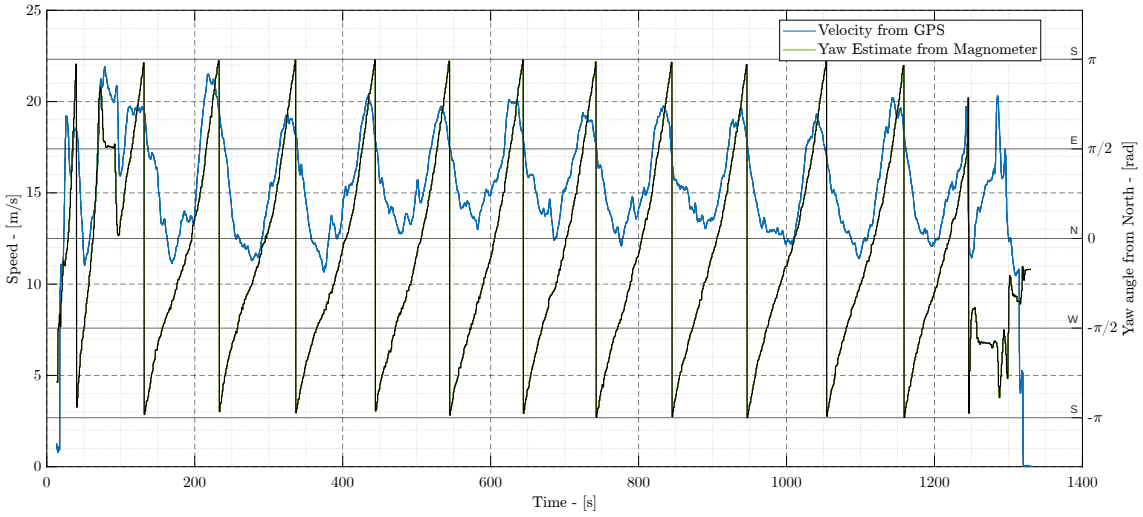

Figure 6.7. Plot of GPS velocity and yaw as $\pm\pi$ for South, 0 being North, $\pi/2$ = East and $-\pi/2$ = West

A "Pseudo Airspeed" is also estimated from the open-source flight controller which can be compared with the FOC estimate, as in Figure 6.8.

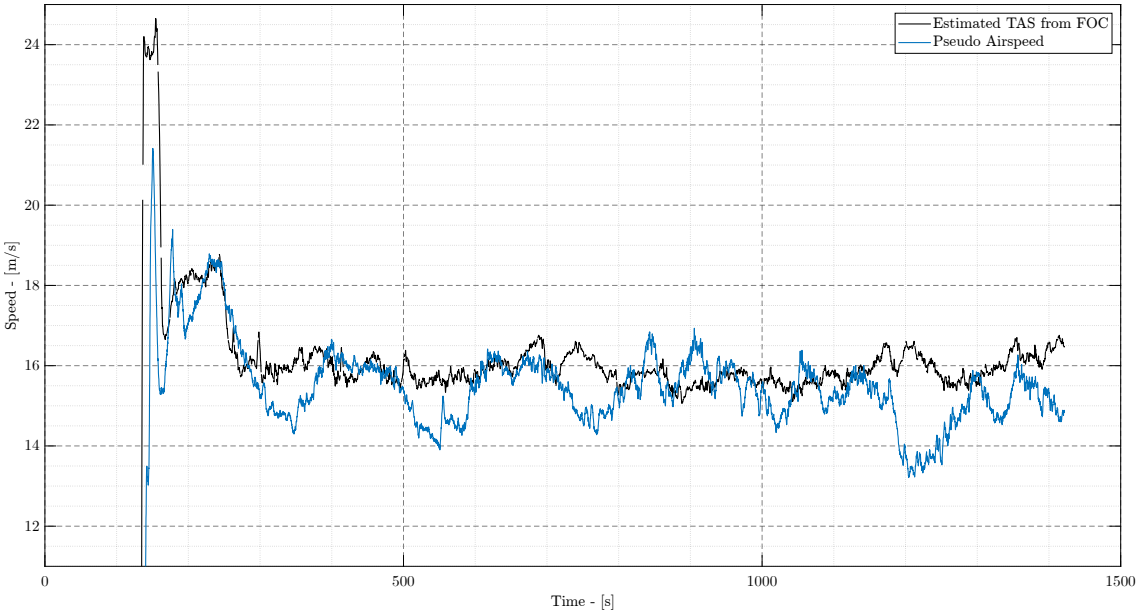

Figure 6.8. Pseudo airspeed and FOC estimate

The error between these two can also be plotted, as in Figure 6.9.

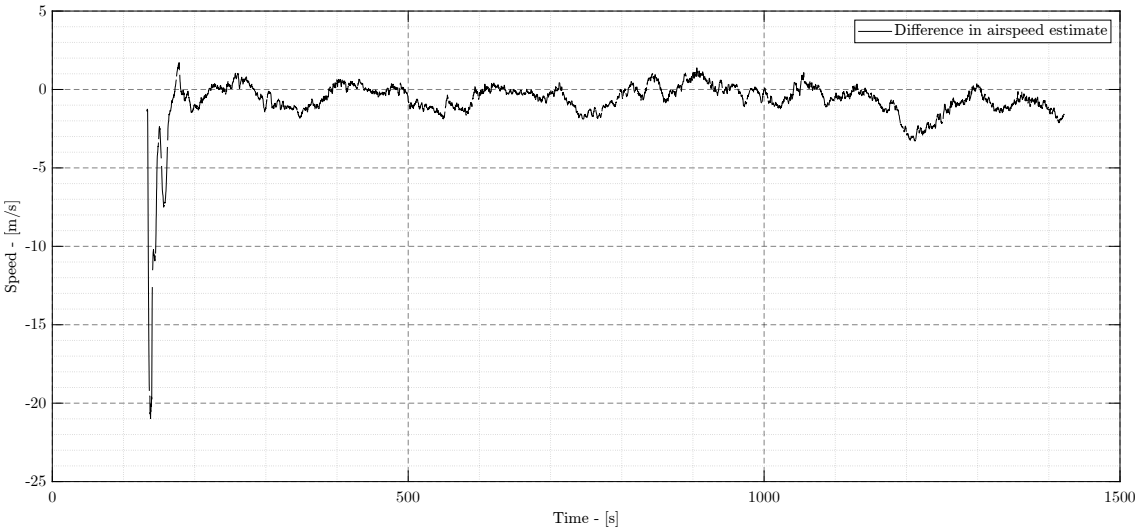

Figure 6.9. Error between Pseudo airspeed and FOC estimate

As shown in Figure 6.9 the estimates differ around 4.5% but are estimates from different sources. The mean difference was 0 73057m/s.

The idea of using FOC states to estimate the airspeed seams viable, yet can not be truly validated without a direct measurement of the dynamic pressure.
To use the airspeed estimate for navigation, an estimate of the wind is necessary, as true airspeed is the sum of ground and wind speeds.
More work is to be done on this estimate for it to be a reliable measure of TAS, as an

example the changes in air density is not considered in the poly-fit at all, but just kept static.
It must also be considered that the "airspeed" gained through the governing equations of motion assumes a relative airflow directly into the propeller disk area, and does not consider air mass change of direction. The exchange of energy as the UAV changes altitude should probably be included in the estimate aswell. For the same reasons this estimate is not expected to be viable for a quad-copter type design.

Discussion 7

As hopefully demonstrated, Aircrafts are multiple-input, multiple-output, nonlinear dynamical systems with complicated, nonlinear, and maybe time-varying aerodynamics. For an aircraft in flight, the applied forces and moments must be calculated from other measurement, and large amounts of data is to be processed. Aircraft measurements can be expected to be noisy and sensors have their practical limitations and own covariance. Also the physical quantities cannot be varied independently for an aircraft in flight. In other words it is not a trivial task to model an aircraft. Simplification of Aerodynamic principals alone can be discussed at length, but will not be in here, however some of the biggest simplifications will be mentioned. Any lift from the fuselage was not included, and is therefore a discrepancy. None of the carryover effects where included, which might be a fair assumption, but has not been proven in anyway. Downwash and elasticity effects of and on the tail of the aircraft was also not included. It was assumed that the relative slow airspeeds and narrow airframe-parts would not cause significant downwash or be subject to sufficient force for bending. There might however very well be a noticeable movement of the entire elevator against the servo arm. The skin friction coefficient estimate was not validated in anyway, but matched regular aircraft values. Again because of the relative slow airspeed, the wetted area of the aircraft was assumed to be the entire aircraft, this was however not validated, but could be done with wind tunnel testing.

The constants k0 and k1 from Equation 4.89 reused from a jet-trainer aircraft and not thoroughly investigated. But as the yaw damping should be a relatively small part of the force input, this was deemed as a sufficient solution for proof of concept.

In the modelling, the table for C_L is used again for several other coefficient, which makes the model quite sensitive to errors in this table. As described the peak angel of attack has to be known, which might not be available.

As mentioned in Chapter 5 System identification is favoured over but often combined with scaled model wind tunnel testing. But in the case of a mini-UAV, a full scale windtunnel test is quite achievable. A wind tunnel test would provide a more controllable environment for testing specific conditions. For example, control surfaces can be deflected while the aircraft is kept at the same attitude.

The validity of the airspeed estimate can be discussed as, essentially, the propeller is just seen as a disk with mass flow through it. The governing equations might be to simplified for the highly dynamic case of flight, with changing airflow angle.

Conclusion 8

Though more is to be done before a usable solution for navigation is complete, this concludes the modelling part. The problem statement for this project was:

How can a fixed-wing mini-UAV be modeled for more confidence in predicting dynamic behaviour than a generic 6DOF rigid body model?

As a secondary objective the following was also be investigated:

What states can be attained by exploiting information from the drivetrain control algorithms, specifically Field Oriented Control on a BLDC?

The following sub-questions where stated:

- How can a parametric model of a mini-UAV be derived from aerodynamic principles and geometric information?
- How are the settings which provide the most efficient cruise flight found?
- How can a mini-UAV be modeled using system identification methods?
- How can FOC variables be used to aid the flight controller?

An aerodynamic model can be constructed to better predict the behaviour of an aircraft compared to a generic 6DOF rigid body model. Two methods for aerodynamic modelling was presented in this project. A parametric model was assembled using 51 physical parameters from the aircraft. Several assumptions, simplifications or estimates where made along the way, and the product of inertia where best guesses. The modeling was done as look up tables for the non-dimensional aerodynamic coefficients, with the intent of interpolating values from the current conditions. This solution works fine for batch processing and simulation, but for real-time implementation, might not be practical as look up tables are not easily included in a statespace model.

An identified system model was also created using flight data, 8 physical parameters and SIDPAC software. The system identification model did not show great accuracy, between 24.5 and 88.9%, due to the physical parameter inaccuracies, disturbances and correlated control inputs from rudder and ailerons.

A method of finding the most efficient trim flight conditions was also derived. For a set airspeed the approach was to minimize the acceleration in x and z directions for the inertial frame as well as pitch rate in the equations of motion.

The concept of using the FOC variables i_q and rotor speed to estimate the airspeed showed promise, but could not be validated by measurements with the current configuration.

Overall both modelling methods required a substantial amount of bookkeeping, and as such introduces a higher risk of error and a requirement for debugging. A crucial point of the modeling in both cases is the determination of the inertia matrix. Unfortunately this was the physical parameter which came with the most uncertainty for this project. Both modeling methods have advantages for different applications, The parametric model can be used for design iterations pre-production, while the system identification offers higher precision.

The obvious next steps is to reshape the derived models into statespace models for use in sensorfusion algorithms, in order to compare the navigational suitability of the models.

Bibliography

[1] Bilal Akin, Manish Bhardwaj, and Jon Warriner. *Trapezoidal Control of BLDC Motors Using Hall Effect Sensors.*

[2] John B. Brandt, Robert W. Deters, Gavin K. Ananda, Or D. Dantsker, and Michael S. Selig. 2015-2022.

[3] Soren Hansen and Mogens Blanke. Diagnosis of airspeed measurement faults for unmanned aerial vehicles. *IEEE Transactions on Aerospace and Electronic Systems*, 50(1):224–239, 2014.

[4] Schlichting Hermann and Truckenbrodt Erich. *Aerodynamics of the airplane.* McGraw-Hill, 1979.

[5] Frank Hitchens. *Propeller Aerodynamics: The History, Aerodynamics Operation of Aircraft Propellers.* Andrews UK Ltd, Luton, Bedfordshire, 1st edition, 2015.

[6] Jonghyuk Kim and Salah Sukkarieh. 6dof slam aided gnss/ins navigation in gnss denied and unknown environments. *Journal of Global Positioning Systems*, 01(9), 2005.

[7] V. Klein and Eugene Morelli. *Aircraft System Identification: Theory And Practice.* 08 2006.

[8] Dr. Christopher W. Lum. *The Flat Earth Equations of Motion.*

[9] Prof. Z. S. Spakovszky MIT. *Thermodynamics and Propulsion.*

[10] PR Newswire. *PR Newswire - Lockheed Martin Awarded Desert Hawk 3 Contract from U.K. Ministry of Defence.*

[11] Mika Okuhara, Torleiv H. Bryne, Kristoffer Gryte, and Tor Arne Johansen. Phased array radio navigation system on uavs: Real-time implementation of in-flight calibration. *IFAC-PapersOnLine*, 56(2):1152–1159, 2023. 22nd IFAC World Congress.

[12] Abhinav Ranjan and Shraddha Prasad. Sinusoids and its orthogonality. In Jayeeta Chattopadhyay, Rahul Singh, and Vandana Bhattacherjee, editors, *Innovations in Soft Computing and Information Technology*, pages 1–6, Singapore, 2019. Springer Singapore.

[13] Dr. Shane Ross. *Rigid Body Kinematics.*

[14] R. F. Stengel. *Flight Dynamics, Second Edition.* Princeton University Press, 2022.

[15] Wikipedia. *Density of air.*

Data A

SIDPAC Standard Data Channels

E.A. Morelli
NASA Langley Research Center
July 28, 2013

CH. NO.	SYMBOLS	DESCRIPTION	UNITS
1	time	time	sec
2	vt	airspeed	ft/s
3	beta	sideslip angle	deg
4	alpha	angle of attack	deg
5	p	roll rate	deg/s
6	q	pitch rate	deg/s
7	r	yaw rate	deg/s
8	phi	Euler roll angle	deg
9	the	Euler pitch angle	deg
10	psi	Euler heading angle	deg
11	ax	x body axis acceleration	g
12	ay	y body axis acceleration	g
13	az	z body axis acceleration	g
14	el	elevator deflection	deg
15	ail	aileron deflection	deg
16	rdr	rudder deflection	deg
17	tef	trailing edge flap deflection	deg
18	lef	leading edge flap deflection	deg
19			
20			
21			
22			
23			
24			
25			
26			
27	qbar	dynamic pressure	lbf/ft^2
28	mach	Mach number	--
29	rho	air density	$slug/ft^3$
30	h	altitude	ft
31	lonstk	longitudinal stick deflection	in
32	latstk	lateral stick deflection	in
33	rudped	rudder pedal deflection	in
34	thtl	throttle	deg
35			
36	pwr	power level	percent
37			
38	thrust	thrust	lbf
39			
40	rpm	rpm	rpm
41			
42	pdot	roll acceleration	deg/s^2
43	qdot	pitch acceleration	deg/s^2
44	rdot	yaw acceleration	deg/s^2

45	xcg	x cg position	in
46	ycg	y cg position	in
47	zcg	z cg position	in
48	mass	aircraft mass	slug
49	Ixx	roll inertia	slug-ft^2
50	Iyy	pitch inertia	slug-ft^2
51	Izz	yaw inertia	slug-ft^2
52	Ixz	x-z cross inertia	slug-ft^2
53	pm	measured roll rate	deg/s
54	qm	measured pitch rate	deg/s
55	rm	measured yaw rate	deg/s
56	axm	measured x body axis acceleration	g
57	aym	measured y body axis acceleration	g
58	azm	measured z body axis acceleration	g
59	betadot	sideslip angle rate	deg/s
60	alphadot	angle of attack rate	deg/s
61	CX	x body axis aerodynamic force coefficient	--
62	CY	y body axis aerodynamic force coefficient	--
63	CZ	z body axis aerodynamic force coefficient	--
64	Cl	aerodynamic rolling moment coefficient	--
65	Cm	aerodynamic pitching moment coefficient	--
66	Cn	aerodynamic yawing moment coefficient	--
67	CD	aerodynamic drag force coefficient	--
68	CYw	wind axis aerodynamic side force coefficient	--
69	CL	aerodynamic lift force coefficient	--
70	CT	thrust force coefficient	--
71	phat	non-dimensional roll rate	--
72	qhat	non-dimensional pitch rate	--
73	rhat	non-dimensional yaw rate	--
74	u	x body axis velocity component	ft/s
75	v	y body axis velocity component	ft/s
76	w	z body axis velocity component	ft/s
77	sarea	wing reference area	ft^2
78	bspan	wing span	ft
79	cbar	mean aerodynamic chord	ft
80	betam	measured sideslip angle	deg
81	alpham	measured angle of attack	deg
82	lon	longitude	deg
83	lat	latitude	deg
84			
85			
86			
87			
88			
89			
90			